Functional Protein Based Materials

Laura E. Hanzly

Dissertation submitted to the faculty of the Virginia Polytechnic Institute and State University in partial fulfillment of the requirements for the degree of

Doctor of Philosophy
In
Biological Systems Engineering

Justin R. Barone, Chair
Chenming (Mike) Zhang
Ryan S. Senger
Charles E. Frazier

June 12 2019
Blacksburg, Virginia

Keywords: Protein, Amyloid, Actuators, Gelatin, Soft Robotics

Functional Protein Based Materials

Laura E. Hanzly

ABSTRACT

The proteins wheat gluten and gelatin were tested for use in biocomposites and soft actuating materials, respectively. In Chapter II, the self-assembly mechanism of trypsin hydrolyzed wheat gluten (THWG) into rigid β-sheets was applied to an aqueous polyvinyl alcohol (PVA) environment. Aqueous PVA was used in order to determine the effects of an aqueous environment other than pure water on THWG self-assembly kinetics and to realize the potential use of THWG as a nanofiller in polymer matrices. THWG was able to self-assemble into anisotropic spikes and agglomerates of spikes called "pompons" through hydrophobic interactions. THWG self-assembly kinetics were retarded in aqueous PVA solutions compared to water, with the highest molecular weight PVA solution showing the slowest self-assembly kinetics. Chapters III and IV explore the potential of gelatin hydrogels for use in soft actuators. A gelatin bilayer system was designed where an active layer swelled more than a passive layer to cause the system to bend/actuate in response to an environmental stimulus. In Chapter III, gelatin layers were chemically crosslinked to different degrees with glutaraldehyde to achieve bilayer bending when placed in water. Curvature of the bilayer system was found to be dependent on the difference in volume swell ratio between the two layers. It was determined that maximum bending occurred when the passive layer swelled to 60% of the swelling of the active layer. Addition of pre-gelatinized starch to the active layer increased layer swelling and bilayer curvature. Treating the starch containing bilayer with α-amylase returned the bilayer to its original shape. In Chapter IV, a pH responsive gelatin bilayer was constructed using Type A and Type B gelatin. Type A and Type B gelatin gels had different chemical properties and swelled to different volumes based on the gel solution pH. Bilayers constructed from Type A and Type B gelatin exhibited different degrees of bending when placed in various pH solutions with maximum curvature occuring at pH 10. A cyclic actuator could be formed when the bent bilayers were placed in a minimum of 0.01M NaCl solution. Placement in salt solution resulted in the unbending of the bilayer. Overall, this work demonstrated the various applications of proteins as functional and green materials.

Functional Protein Based Materials

Laura E. Hanzly

GENERAL AUDIENCE ABSTRACT

The majority of plastics consist of synthetic polymers derived from oil that cannot be broken down by the environment (i.e., not biodegradable). Research is underway to develop sustainable, biodegradable materials. Proteins are a biological polymer that have a wide range of chemical, structural, and functional properties; for this reason they are an excellent source material for use in the design of environmental friendly materials. In Chapter II, the ability of wheat gluten protein to self-assemble into rigid, nanosized structures is used to explore the potential of the protein to be used as a biodegradable nanofiller. A nanofiller is added to various materials in order to improve the overall mechanical properties of the material. Wheat gluten is self-assembled in an aqueous polymer environment. The results show that the polymer environment stunts or slows down the self-assembly rate of the protein compared to a pure water enivronment. Nanometer sized spikes form in the polymer solutions, indicating wheat gluten could be used as a nanofiller in certain materials. Chapters III and IV explore the use of gelatin proteins for applications in soft robotics. Soft robots and their moveable parts, called soft actuators, are deformable and respond to changes in the environment such as pH, light, temperature, etc. For this reason, soft robots are considerable adaptable compared to traditional rigid robots. Designing a soft actuator from gelatin gels would result in a "smart" material that is biocompatible and biodegradable. A gelatin soft actuator is created using a bilayer design in which one layer of the bilayer swells more than the other layer causing the entire system to bend/actuate. Depending on how the bilayer system was fabricated, bending could be achieved based on stimuli such as the presence of water, the presence of a substrate and enzyme, and changes in pH. Overall, this dissertation demonstrates the extraordinary potential for the use of proteins in designing sustainable materials.

ACKNOWLEDGEMENTS

I would like to thank my advisor Dr. Justin Barone for his guidance and mentorship. I would also like to thank my committee members for their feedback and service on my committee.

I cannot thank my family and friends enough for their never ending support. Thank you Allyson for always listening to my never ending worries and thank you Leo for always being there by my side.

TABLE OF CONTENTS

ABSTRACT....ii

GENERAL AUDIENCE ABSTRACT iii

ACKNOWLEDGEMENTS....iv

TABLE OF CONTENTS v

LIST OF FIGURES....vi

LIST OF TABLES x

ATTRIBUTIONS....xi

CHAPTER 1: INTRODUCTION 1

REFERENCES…….... 6

CHAPTER 2: PROTEIN AGGREGATION IN AQUEOUS POLYVINYL ALCOHOL SOLUTIONS 11

REFERENCES…… 34

CHAPTER 3: GELATIN HYDROGEL BILAYER ACTUATORS 38

REFERENCES…… 60

CHAPTER 4: PH RESPONSIVE CYCLIC GELATIN ACTUATORS 63

REFERENCES…… 76

CHAPTER 5: CONCLUSIONS 78

LIST OF FIGURES

CHAPTER 2

Figure 1. Comparing the ratio of the symmetric CH_3 deformation to the asymmetric CH_3 deformation, $\delta_s(CH_3)/\delta_{as}(CH_3)$, quantifies the level of hydrophobic interactions during self-assembly (a). Included for comparison is the pure THWG protein in aqueous solution.[37] Comparison of hydrophobic interactions versus reduced time, in hours, shows kinetics of self-assembly are similar across solutions (b).....20

Figure 2. Pure PVA controls show no regular surface features when incubated under the same conditions as the samples with protein. 22

Figure 3. An example of a self-assembled protein "spike". The spike widths remain 200-350 nm throughout the process. 22

Figure 4. SEM image of spikes and unassembled surrounding material. The black arrow points to a region that appears different than the material in the rest of the image and could point to unassembled protein or PVA. 23

Figure 5. Images of agglomeration of protein spikes in THWG:31k g/mol PVA composites. (a) Brightfield microscopy of a 6 □m thick cross section of THWG:31k g/mol PVA composite. (b) Protein aggregates fluoresce green when stained with Thioflavin-T, indicative of β-sheet structure. (c) SEM of the same portion of cross section observed in (a) and (b). Fully spherical spiked agglomerates or "pompons" are present as well as partially formed pompons. (d) Close up of pompon. Arrows in images indicate location of pompon observed in (d).....24

Figure 6. Pompon diameter does not vary with time or solution viscosity. 25

Figure 7. Pompons appear, maximize their number, then slowly disappear with time. The first point in time for each sample indicates the initial observance of spikes (Table I). 27

Figure 8. Molecular model based on SEM and DSC results showing possible morphologies for THWG:PVA composites. 29

Figure 9. dTGA results for PVA control and THWG:PVA composites. 29

Figure S1. Viscosity measurements with increasing shear rate for each of three different M_W PVA solutions. 31
Figure S2. The extent of hydrophobic interactions, $\delta_s(CH_3)/\delta_{as}(CH_3)$, correlates with the amount of protein β-sheets in the THWG:PVA composites. 31
Figure S3. Anisotropic spike width is invariant with self-assembly time and medium viscosity. Sample data is missing from select time points due to lack of available spikes at an appropriate angle to accurately measure spike width. 32
Figure S4. Additional photos of pompons observed in protein-PVA samples. 32
Figure S5. Glass transition temperature (T_g) from second DSC heating scan. 33
Figure S6. Melting behavior from DSC second heating scan. 33

CHAPTER 3

Figure 1. Gelatin bilayer actuating mechanism. Differences in crosslinking cause unequal volume swelling between layers resulting in bilayer bending towards the higher crosslinked side. The higher crosslinked side is the "passive" layer and the lower crosslinked side is the "active" layer in the bilayer. 44
Figure 2. Gelatin storage modulus, G', and volume swell ratio, Q, as a function of GTA solution concentration used for crosslinking. 48
Figure 3. Gelatin bilayer bending over time. Bilayers are allowed to swell for a total period of 48 hours. Bending between 24-48 hrs. is not significant enough to include a picture. GTA "1/0.05" bilayer shown. 48
Figure 4. Average curvature for each bilayer. Pictures on graph show actual bending for that particular bilayer. The GTA concentration of each Q_p/Q_a value can be referenced in Table S1. 50
Figure 5. (a) Starch addition to active layer of "1/0.05" gelatin bilayer results in increased curvature. (b) 1/0.05 gelatin bilayer (left), 1/(0.05 +30% starch) bilayer (middle), and (1/0.05 + 50% starch) bilayer (right). The active layer is on the bottom and is more opaque than the passive top layer. 52
Figure 6. Gelatin bilayers that display no curvature will bend with the incorporation of starch into the active layer. 50% starch is added to the active layer of 0.125/0.0125 bilayers. The starch filled bilayers demonstrate significant bending compared to the

0.125/0.0125 starch-free bilayers. Treating the starch-gelatin bilayers with α-amylase eliminates the increase in curvature caused by starch. 53

Figure 7. (a) 1/(0.05 + 50% starch) bilayers treated with α-amylase. The presence of α-amylase results in decreased bilayer curvature and weight. "No α-amylase" group consists of 1/(0.05 + 50% starch) bilayers not treated with α-amylase but still swollen in deionized water for the same amount of time as the "α-amylase" group. The "no α-amylase" group does not show a decrease in weight or curvature. (b) Visual of curvature change of 1/(0.05 + 50% starch) bilayer after α-amylase treatment. 54

Figure S1. Example of fabrication and nomenclature of gelatin control layer (top) and bilayer (bottom). For the control layer, the name denotes what GTA percentage crosslinked the layer. For example, "2/0.2" indicates that the gelatin layer was first crosslinked with 2% GTA for 30 minutes and then crosslinked with 0.2% GTA for another 30 minutes to form the "2/0.2" control layer (top). Bilayer name indicates the crosslinking of the passive and active layers together. For the bilayer "2/0.2", the passive layer was first crosslinked with 2% GTA and then the active and passive layers were crosslinked together in 0.2% GTA to form a bilayer consisting of a passive layer crosslinked with both 2% and 0.2% GTA and an active layer crosslinked with 0.2% GTA (bottom). Data included in Table S1. 57

Figure S2. (a) Swelling difference between 0.05 gelatin single layer and (0.05 +50% starch) gelatin single layer. Starch incorporation increases the equilibrium swelling ratio, Q_a, of the active layer. (b) Starch incorporation into single gelatin layers does not result in bending. 58

Figure S3. Starch-free 1/0.05 gelatin bilayer subjected to α-amylase treatment. α-amylase does not change the weight of 1/0.05 bilayers indicating the enzyme is not breaking down gelatin. 58

CHAPTER 4

Figure 1. Schematic of bilayer actuator design. The active layer (gray layer) swells more than the passive layer (white layer) causing the entire system to bend. Bending is quantified by measuring the radius of curvature, R_c. 67

Figure 2. Average volume swelling ratio, Q, of Type A and Type B gelatin layers at various pH. 70

Figure 3. Curvature of bilayers at various pH. (a) Pictures of gelatin bilayers swollen for 48 hours at pH 6, 9, and 10. (b) Average curvature for bilayers after 48 hours of swelling in different pH solutions. Q_p/Q_a is the volume swell ratio of the passive layer compared to the active layer. For pH values 4,6, and 8, Type A gelatin swells more than Type B and is used as the active layer in calculations. At pH 10, Type B gelatin is the active layer because it swells more than the Type A layer. 72

Figure 4. Cyclic actuation of gelatin bilayers. Gelatin bilayers are first swollen in pH=6 where they are relatively flat. Bilayers are then placed at pH=10 where they show maximum curvature. Bilayers are then placed in either 0.1M, 0.05M, or 0.01M NaCl solutions so the individual layers contract and the bilayer unbends. Finally, bilayers are placed back into pH=10 solutions. The control group was kept in a constant solution of pH=10. 74

LIST OF TABLES

CHAPTER 2

Table 1. Viscosities of PVA control solutions. 21

Table 2. Characteristic time points in pompon formation as observed in SEM and FTIR. 27

Table 3. Thermal properties of PVA control and THWG:PVA composites. 28

CHAPTER 3

Table S1. Swelling ratios for individual layers and Q_p/Q_a for bilayers. Control and bilayers are named in accordance with the system described in Figure S1. 59

CHAPTER 4

Table 1. Properties of Type A and Type B Gelatin. 71

ATTRIBUTIONS

Dr. Justin R. Barone contributed to the overall experimental design, data analysis, and writing of manuscripts in Chapters 2-4.

Barbara L. DeButts, of the Macromolecules Innovation Institute and Macromolecular Sceince and Engineering at Virginia Tech, devised and executed experiments featured in Chapter 2.

Danielle Shell, while participating in the Interdisciplinary Science and Engineering Program at Virginia Tech, performed experiments included in Chapter 2.

Kristofer A. Krisofferson, while participating in the NSF Research Experience for Undergraduates (REU): "Food-Energy-Water Systems" at Virginia Tech, performed experiments included in Chapter 3.

I would like to thank each of the co-authors for their contributions this research.

CHAPTER 1: INTRODUCTION

1.1 Overview

Demand is increasing for the development of novel materials that incorporate natural, biological components into their structure in order to produce materials that are biocompatible, biodegradable, and sustainable. Synthetic materials and polymers, such as polyethylene and polypropylene, have dominated the materials industry due to their outstanding mechanical properties and relatively low cost. However these synthetic materials come with a significant environmental burden; synthetic polymers are often derived from crude oil and accumulate and persist in the environment due to their lack of biodegradability.[1, 2] It is predicted that by the year 2050 approximately 12,000 metric tons (Mt) of plastic waste will occupy landfills and the natural environment[3]. In order to shift society away from a reliance on oil-based products as well as reduce environmental waste, alternative materials created from biological, renewable materials must be developed.

Proteins exhibit an assortment of chemical, bioactive, and structural properties and functions.[4] Proteins are polymers, comprised of sequences of amino acids that give rise to unique protein secondary, tertiary, and quaternary structures. This array of functional and structural properties along with their intrinsic biodegradability makes proteins well suited for biomaterials and composite biomaterials applications. Traditional examples of protein-based materials include silk and wool[5], but current research focuses on the use of proteins for applications such as the creation of green materials[4], as a biological filler in polymer composites[6] and in the design of "smart" polymeric materials[7]. Examples include plastics derived from soy protein[8], the use of lysozyme protein as reinforcement in polydimethylsiloxane (PDMS)[9], and a smart material made from calmodulin[10]. All of these examples not only showcase the potential for proteins for use in various materials applications, but also demonstrate the ability to design new materials that are not based purely on synthetic polymers.

In this research, proteins are used to develop novel biocomposites and smart materials: 1) wheat gluten (WG) protein is used as a nanofiller in polyvinyl alcohol (PVA) and 2) gelatin proteins are utilized in the development of smart and soft actuators.

1.2.1 Nanocomposites and Biological Fillers

Nanocomposites are nanometer-sized fillers dispersed in polymers in order to increase the mechanical and barrier properties of the polymer matrix.[11] Nanofillers have a large surface area so there is a large amount of interaction with the polymer matrix. These fillers are often used in low concentration in order to minimize nanofiller agglomeration; separating and dispersing nanofillers is a challenge for industrial manufacturing.[12, 13] *In situ* polymerization, in which nanofiller is first mixed with monomers and then the monomers are polymerized to form the polymer matrix, has been proposed as a solution to the challenge of nanofiller dispersion. However this process can only be done with certain polymers and cannot be applied to large-scale production.[14-16]

Fillers derived from biological components are lightweight, sustainable, and are often low cost because they are diverted from agricultural waste streams.[17] In order for a biological filler to be applicable to industry, it must outperform and be low cost compared to synthetic fillers. The use of biological fillers such as natural fibers have long been used in composites, however natural fibers show poor fiber/matrix interactions, water resistance, and poor durability.[18] Nanocellulose has also been used as a biological filler, however it is not yet efficient or economical to use as a reinforcing material in composites.[19] Additionally, biological fillers are sensitive to temperature degradation, which restricts the processing conditions and polymer matrices they are compatible with.[20, 21]

1.2.2 Amyloids and β-sheet structure

Proteins are able to form rigid, nanoscale structures. The secondary structures of proteins can form α-helices, β-sheets, or random coils.[22] β-sheets arise through hydrogen bonding of the main chain carbonyl (-C=O) on one amino acid to the main chain secondary amine (-NH) on another amino acid. β-sheets are characterized by a protein inter-chain distance

of approximately 0.47 nm and their assemblies are rigid and extremely stable.[23, 24] In some cases, β-sheets can elongate and stack together, eventually forming nanometer sized protofibrils and micron size fibers.[25-27] Proteins can be induced to form β-sheet structures by denaturing (i.e., unfolding) the protein using high temperature, pH, salt, detergents, or applied stress. In aqueous solution, the hydrophobic groups on the amino acids of the protein will be thermodynamically driven together to form β-sheets.[28, 29] This process of proteins aggregating into supramolecular structures is termed protein self-assembly.

Fibers and protofibrils in which β-sheets sheets have assembled perpendicular to the fiber axis are known as amyloids.[30-33] Amyloids are commonly known for their pathogenic role in neurodegenerative diseases such as Alzheimer's Disease and Huntington's Disease.[31, 34] However examples of "functional" amyloids exist in nature such as the egg stalks of *Chrysopidae*[35] and the adhesive cement barnacles use to attach to rocks[36]. Amyloid fibers can have a Young's modulus comparable to silk and an ultimate strength comparable to steel.[37] These outstanding properties render amyloid forming proteins ideal candidates for use in biomaterials and composites.

1.2.3 Self-Assembly Mechanism of Wheat Gluten Protein

Wheat gluten is a mixture of gliadin and glutenin proteins.[38] It has been previously shown that enzymatic hydrolysis of wheat gluten via trypsin results in protein fragments with molecular weights less than 10,000 g/mol.[39, 40] The hydrophobic groups on the short peptide side chains self-assemble into β-sheets when placed in water.[41] When left incubating at near physiological conditions (37°C, pH 8), the protein fragments will continue to self-assemble into micron sized amyloid fibers.[27] This makes trypsin hydrolyzed wheat gluten (THWG) an interesting protein mixture to study, as it has the ability to form nanoscale β-sheet structures as well as micron-sized fibers depending on the environmental conditions the hydrolyzed protein is exposed to. Prior to this research, THWG has only been self-assembled in a pure water environment, the effect of the presence of other macromolecules in solution on the self-assembly kinetics of THWG has yet to be studied.

1.2.4 Self Assembly of Trypsin Hydrolyzed Wheat Gluten in Polyvinyl Alcohol (PVA)

To overcome the challenges associated with nanofiller dispersal into a polymer matrix, trypsin hydrolyzed wheat gluten proteins are self-assembled in an aqueous polar, polymer solution. Polyvinyl alcohol is used as the polymer because it is polar, water soluble, and has packaging applications.[42] It is hypothesized that the wheat gluten proteins will self-assemble into β-sheets within the polymer solution, thereby creating a nanofiller phase through *in situ* nanofiller formation. A THWG nanofiller would be environmentally friendly, bio-based, and biodegradable and overall produce a "green" composite compared to synthetic nanofillers.

As mentioned earlier, THWG has previously been self-assembled in pure water solutions. Other researchers have tested protein aggregation carried out in aqueous hexafluoro isopropanol (HFIP) and trifluoroethanol (TFE). At higher concentrations of HFIP or TFE in water, there is a sufficiently hydrophobic environment such that β-sheet structures do not self-assemble.[43] However, at low TFE concentration, protofibril formation is thermodynamically favored at faster rates in the same protein concentration regime where only unstructured aggregates or protofibrils form slowly in water.[44] These results show that the characteristics of the surrounding environment can have a profound effect on protein self-assembly. In this work, the inter-molecular interactions, kinetics, and morphology of THWG self-assembly in aqueous PVA is examined.

1.3.1 Soft Robotics and Soft Actuators

The robotics industry has been dominated by the development of rigid machines designed to perform specific and precise tasks based on some form of user input. However, the need for machines that are flexible and adaptable to changes in environment has lead to the emerging field of soft robotics.[45-47] Soft robots are elastically deformable, allowing them to absorb energy and move based on external stimuli. Not only are soft robots adaptable compared to rigid-bodied robots, they also offer the advantage of being safer in terms of human interaction due to their compliant nature.

The continued development of soft robotics relies on the design and fabrication of novel sensors and soft actuators.[45, 48] Soft actuators respond to environmental fluctuations in pH, solvent, heat, humidity, electric field, light, etc., resulting in the conversion of chemical/physical energy into mechanical work.[49] Soft actuators can be constructed from natural or synthetic elastomeric materials, current examples include shape-memory polymers[50], ionic liquids and polymers[51-53], polyelectrolyte gels[54], and electroactive polymers[55]. The implementation of these materials into actuator designs often requires expensive and tedious processing conditions such as lithography, multi-material 3D printing, and shape deposition manufacturing (SDM).[46] Additionally, few soft actuator designs incorporate a material that is biodegradable[56], opting instead to use nonrenewable synthetic polymers. Finding a low cost, sustainable material that can be easily manipulated as well as mass-producible for soft actuation is a current challenge for commercial applications of soft robots.

1.3.2 Properties of Gelatin Hydrogels

Gelatin is an inexpensive and widely available mixture of proteins derived from collagen found in animal skin. Because it is biodegradable and biocompatible, gelatin has been utilized in a variety of pharmaceutical and biomedical applications.[57-59] A valuable property of gelatin is its ability to form physically-crosslinked hydrogels when placed in hot water. Hydrogels are advantageous in terms of materials applications because they have the ability to swell to large volumes when placed in water.[60] Therefore hydrogels can produce macroscopic actuation as a result of swelling and/or shrinking.[61] Additionally, the degree of swelling, modulus, and stability of gelatin hydrogels can be controlled through chemical crosslinking of the gels.[62] A high degree of crosslinking within the gelatin hydrogel causes the gel to be stiff and exhibit a low degree of swelling.

1.3.3 Gelatin Hydrogel Soft Actuator Design

A solution to the commercial viability of soft actuators may lie in hydrogels, specifically gelatin hydrogels. Gelatin is an ideal polymeric material for use in soft actuator design as it can easily be manipulated, poured into molds, and cross-linked to various degrees resulting in a range of mechanical properties when swollen in water. Soft Actuators

designed from gelatin would also be completely biocompatible and biodegradable, offering a 'green' alternative to the use of nonbiodegradable synthetic materials. Indeed, a soft "edible" robot has been created from gelatin[63], however the actuation of this robot relies on user input in the form of injected pressurized air.

In this work we present a gelatin hydrogel bilayer soft actuator design that bends in response to changes in the environment such as the presence of water, the presence of an enzyme, and changes in pH. The soft actuator is comprised of two gelatin layers; the layers are fabricated such that one layer swells more than the other layer in response to a stimulus causing the entire bilayer to actuate (i.e., bend). This type of actuator design is not new, as examples of bilayer soft actuators exist in nature. For example, the opening and closing of pine cones in response to the presence of water is due to the bilayer structure of the individual scales on the pine cone.[64] Bilayer actuators from synthetic polymers have also been designed[65, 66], however as previously stated these actuators are often tedious and expensive to fabricate in addition to not being biodegradable. Exploring the feasibility of soft actuators designed from gelatin will aid in the shift towards using environmentally friendly polymers for material design.

References

1. Tokiwa, Y.; Calabia, B. P.; Ugwu, C. U.; Aiba, S., Biodegradability of plastics. *Int J Mol Sci* **2009,** 10, (9), 3722-3742.
2. Zheng, Y.; Yanful, E. K.; Bassi, A. S., A Review of Plastic Waste Biodegradation. *Critical Reviews in Biotechnology* **2005,** 25, (4), 243-250.
3. Geyer, R.; Jambeck, J. R.; Law, K. L., Production, use, and fate of all plastics ever made. *Sci Adv* **2017,** 3, (7), e1700782-e1700782.
4. Hu, X.; Cebe, P.; Weiss, A. S.; Omenetto, F.; Kaplan, D. L., Protein-based composite materials. *Materials today* **2012,** 15, (5), 208-215.
5. Abascal, N. C.; Regan, L., The past, present and future of protein-based materials. *Royal Society Open Biology* **2018,** 8, (10), 180113.
6. Wang, F.; Yang, C.; Hu, X. In *Advanced protein composite materials*, 2014, pp 177-208.
7. Roy, I.; Gupta, M. N., Smart polymeric materials: emerging biochemical applications. *Chemistry & biology* **2003,** 10, (12), 1161-1171.
8. Kumar, R.; Choudhary, V.; Mishra, S.; Varma, I. K.; Mattiason, B., Adhesives and plastics based on soy protein products. *Industrial crops and products* **2002,** 16, (3), 155-172.

9. Oppenheim, T.; Knowles, T. P. J.; Lacour, S. P.; Welland, M. E., Fabrication and characterisation of protein fibril–elastomer composites. *Acta biomaterialia* **2010,** 6, (4), 1337-1341.
10. Sui, Z.; King, W. J.; Murphy, W. L., Dynamic materials based on a protein conformational change. *Advanced Materials* **2007,** 19, (20), 3377-3380.
11. Tang, X. Z.; Kumar, P.; Alavi, S.; Sandeep, K. P., Recent advances in biopolymers and biopolymer-based nanocomposites for food packaging materials. *Critical reviews in food science and nutrition* **2012,** 52, (5), 426-442.
12. Pavlidou, S.; Papaspyrides, C. D., A review on polymer–layered silicate nanocomposites. *Progress in polymer science* **2008,** 33, (12), 1119-1198.
13. Ray, S. S.; Okamoto, M., Polymer/layered silicate nanocomposites: a review from preparation to processing. *Progress in polymer science* **2003,** 28, (11), 1539-1641.
14. Ou, Y.; Yang, F.; Yu, Z. Z., A new conception on the toughness of nylon 6/silica nanocomposite prepared via in situ polymerization. *Journal of Polymer Science Part B: Polymer Physics* **1998,** 36, (5), 789-795.
15. Zeng, C.; Lee, L. J., Poly (methyl methacrylate) and polystyrene/clay nanocomposites prepared by in-situ polymerization. *Macromolecules* **2001,** 34, (12), 4098-4103.
16. Sun, T.; Garces, J. M., High-Performance Polypropylene–Clay Nanocomposites by In-situ Polymerization with Metallocene/Clay Catalysts. *Advanced Materials* **2002,** 14, (2), 128-130.
17. Rwawiire, S.; Tomkova, B.; Militky, J.; Jabbar, A.; Kale, B. M., Development of a biocomposite based on green epoxy polymer and natural cellulose fabric (bark cloth) for automotive instrument panel applications. *Composites Part B: Engineering* **2015,** 81, 149-157.
18. Saba, N.; Tahir, P.; Jawaid, M., A review on potentiality of nano filler/natural fiber filled polymer hybrid composites. *Polymers* **2014,** 6, (8), 2247-2273.
19. Bharimalla, A. K.; Deshmukh, S. P.; Vigneshwaran, N.; Patil, P. G.; Prasad, V., Nanocellulose-polymer composites for applications in food packaging: Current status, future prospects and challenges. *Polymer-Plastics Technology and Engineering* **2017,** 56, (8), 805-823.
20. Holbery, J.; Houston, D., Natural-fiber-reinforced polymer composites in automotive applications. *Jom* **2006,** 58, (11), 80-86.
21. Espinach, F. X.; Granda, L. A.; Tarrés, Q.; Duran, J.; Fullana-i-Palmer, P.; Mutjé, P., Mechanical and micromechanical tensile strength of eucalyptus bleached fibers reinforced polyoxymethylene composites. *Composites Part B: Engineering* **2017,** 116, 333-339.
22. Wang, Y.; Mao, H.; Yi, Z., Protein secondary structure prediction by using deep learning method. *Knowledge-Based Systems* **2017,** 118, 115-123.
23. Makin, O. S.; Sikorski, P.; Serpell, L. C., Diffraction to study protein and peptide assemblies. *Current opinion in chemical biology* **2006,** 10, (5), 417-422.
24. Serpell, L. C.; Smith, J. M., Direct visualisation of the β-sheet structure of synthetic Alzheimer's amyloid. *Journal of molecular biology* **2000,** 299, (1), 225-231.
25. Bolisetty, S.; Adamcik, J.; Mezzenga, R., Snapshots of fibrillation and aggregation kinetics in multistranded amyloid β-lactoglobulin fibrils. *Soft Matter* **2011,** 7, (2), 493-499.

26. Lara, C.; Adamcik, J.; Jordens, S.; Mezzenga, R., General self-assembly mechanism converting hydrolyzed globular proteins into giant multistranded amyloid ribbons. *Biomacromolecules* **2011,** 12, (5), 1868-1875.
27. Ridgley, D. M.; Barone, J. R., Evolution of the amyloid fiber over multiple length scales. *ACS nano* **2013,** 7, (2), 1006-1015.
28. Eisenberg, D.; Weiss, R. M.; Terwilliger, T. C.; Wilcox, W. In *Hydrophobic moments and protein structure*, 1982, Royal Society of Chemistry: pp 109-120.
29. Eisenberg, D.; Wilcox, W.; McLachlan, A. D., Hydrophobicity and amphiphilicity in protein structure. *Journal of cellular biochemistry* **1986,** 31, (1), 11-17.
30. Chiti, F.; Dobson, C. M., Protein misfolding, functional amyloid, and human disease. *Annu. Rev. Biochem.* **2006,** 75, 333-366.
31. Dobson, C. M., Protein misfolding, evolution and disease. *Trends in biochemical sciences* **1999,** 24, (9), 329-332.
32. Dobson, C. M., Protein folding and misfolding. *Nature* **2003,** 426, (6968), 884.
33. Dobson, C. M.; Šali, A.; Karplus, M., Protein folding: a perspective from theory and experiment. *Angewandte Chemie International Edition* **1998,** 37, (7), 868-893.
34. Blanco, L. P.; Evans, M. L.; Smith, D. R.; Badtke, M. P.; Chapman, M. R., Diversity, biogenesis and function of microbial amyloids. *Trends in microbiology* **2012,** 20, (2), 66-73.
35. Parker, K. D.; Rudall, K. M., Structure of the silk of chrysopa egg-stalks. *Nature* **1957,** 179, (4566), 905-906.
36. Barlow, D. E.; Dickinson, G. H.; Orihuela, B.; Kulp Iii, J. L.; Rittschof, D.; Wahl, K. J., Characterization of the adhesive plaque of the barnacle Balanus amphitrite: amyloid-like nanofibrils are a major component. *Langmuir* **2010,** 26, (9), 6549-6556.
37. Velikov, K. P.; Koenderink, G.; Bonn, M., Amyloids: From molecular structure to mechanical properties. *Polymer* **2013,** 54, (247), 3e2488.
38. Shewry, P. R.; Tatham, A. S.; Forde, J.; Kreis, M.; Miflin, B. J., The classification and nomenclature of wheat gluten proteins: a reassessment. *Journal of cereal science* **1986,** 4, (2), 97-106.
39. Athamneh, A. I.; Barone, J. R., Enzyme-mediated self-assembly of highly ordered structures from disordered proteins. *Smart Materials and Structures* **2009,** 18, (10), 104024.
40. Tuck, C. S.; Latham, A.; Lee, P. W.; Barone, J. R., Wheat gluten plasticized with its own hydrolysate. *Journal of Polymers and the Environment* **2014,** 22, (4), 430-438.
41. Ridgley, D. M.; Ebanks, K. C.; Barone, J. R., Peptide mixtures can self-assemble into large amyloid fibers of varying size and morphology. *Biomacromolecules* **2011,** 12, (10), 3770-3779.
42. Chiellini, E.; Corti, A.; D'Antone, S.; Solaro, R., Biodegradation of poly (vinyl alcohol) based materials. *Progress in Polymer science* **2003,** 28, (6), 963-1014.
43. Crescenzi, O.; Tomaselli, S.; Guerrini, R.; Salvadori, S.; D'Ursi, A. M.; Temussi, P. A.; Picone, D., Solution structure of the Alzheimer amyloid β-peptide (1–42) in an apolar microenvironment. *European Journal of Biochemistry* **2002,** 269, (22), 5642-5648.
44. Fezoui, Y.; Teplow, D. B., Kinetic Studies of Amyloid β-Protein Fibril Assembly. *Journal of Biological Chemistry* **2002,** 277, (40), 36948-36954.
45. Majidi, C., Soft robotics: a perspective—current trends and prospects for the future. *Soft Robotics* **2014,** 1, (1), 5-11.

46. Rus, D.; Tolley, M. T., Design, fabrication and control of soft robots. *Nature* **2015,** 521, (7553), 467.
47. Trivedi, D.; Rahn, C. D.; Kier, W. M.; Walker, I. D., Soft robotics: Biological inspiration, state of the art, and future research. *Applied bionics and biomechanics* **2008,** 5, (3), 99-117.
48. She, Y.; Li, C.; Cleary, J.; Su, H.-J., Design and fabrication of a soft robotic hand with embedded actuators and sensors. *Journal of Mechanisms and Robotics* **2015,** 7, (2), 021007.
49. Asaka, K.; Okuzaki, H., Soft Actuators. *Stretchable Electronics* **2012**, 305-324.
50. Lendlein, A.; Behl, M.; Hiebl, B.; Wischke, C., Shape-memory polymers as a technology platform for biomedical applications. *Expert review of medical devices* **2010,** 7, (3), 357-379.
51. Armand, M.; Endres, F.; MacFarlane, D. R.; Ohno, H.; Scrosati, B., Ionic-liquid materials for the electrochemical challenges of the future. In *Materials For Sustainable Energy: A Collection of Peer-Reviewed Research and Review Articles from Nature Publishing Group*, World Scientific: 2011; pp 129-137.
52. Jager, E. W. H.; Smela, E.; Inganäs, O., Microfabricating conjugated polymer actuators. *Science* **2000,** 290, (5496), 1540-1545.
53. Yang, W.; Choi, H.; Choi, S.; Jeon, M.; Lee, S.-Y., Carbon nanotube–graphene composite for ionic polymer actuators. *Smart Materials and Structures* **2012,** 21, (5), 055012.
54. Glazer, P. J.; Van Erp, M.; Embrechts, A.; Lemay, S. G.; Mendes, E., Role of pH gradients in the actuation of electro-responsive polyelectrolyte gels. *Soft Matter* **2012,** 8, (16), 4421-4426.
55. Pelrine, R.; Kornbluh, R.; Pei, Q.; Joseph, J., High-speed electrically actuated elastomers with strain greater than 100%. *Science* **2000,** 287, (5454), 836-839.
56. Laschi, C.; Mazzolai, B.; Cianchetti, M., Soft robotics: Technologies and systems pushing the boundaries of robot abilities. *Sci. Robot* **2016,** 1, (1), eaah3690.
57. Tabata, Y.; Ikada, Y., Protein release from gelatin matrices. *Advanced drug delivery reviews* **1998,** 31, (3), 287-301.
58. Arvanitoyannis, I. S., Formation and properties of collagen and gelatin films and coatings. In *Protein-based films and coatings*, CRC Press: 2002; pp 289-318.
59. Djagny, K. B.; Wang, Z.; Xu, S., Gelatin: a valuable protein for food and pharmaceutical industries. *Critical reviews in food science and nutrition* **2001,** 41, (6), 481-492.
60. Ganji, F.; Vasheghani, F. S.; Vasheghani, F. E., Theoretical description of hydrogel swelling: a review. **2010**.
61. Ionov, L., Biomimetic hydrogel-based actuating systems. *Advanced Functional Materials* **2013,** 23, (36), 4555-4570.
62. Bigi, A.; Cojazzi, G.; Panzavolta, S.; Rubini, K.; Roveri, N., Mechanical and thermal properties of gelatin films at different degrees of glutaraldehyde crosslinking. *Biomaterials* **2001,** 22, (8), 763-768.
63. Shintake, J.; Sonar, H.; Piskarev, E.; Paik, J.; Floreano, D. In *Soft pneumatic gelatin actuator for edible robotics*, 2017, IEEE: pp 6221-6226.
64. Reyssat, E.; Mahadevan, L., Hygromorphs: from pine cones to biomimetic bilayers. *Journal of the Royal Society Interface* **2009,** 6, (39), 951-957.

65. Stoychev, G.; Turcaud, S.; Dunlop, J. W. C.; Ionov, L., Hierarchical multi-step folding of polymer bilayers. *Advanced Functional Materials* **2013,** 23, (18), 2295-2300.
66. Dai, M.; Picot, O. T.; Verjans, J. M. N.; de Haan, L. T.; Schenning, A. P. H. J.; Peijs, T.; Bastiaansen, C. W. M., Humidity-responsive bilayer actuators based on a liquid-crystalline polymer network. *ACS applied materials & interfaces* **2013,** 5, (11), 4945-4950.

CHAPTER 2: PROTEIN AGGREGATION IN AQUEOUS POLYVINYL ALCOHOL SOLUTIONS

Hanzly, L.E., DeButts, B.L., Shell, D., and Barone, J.R., (2019). *Green Materials* (submitted for review).

Chapter 2 has been submitted to *Green Materials*, a peer-reviewed journal published by the Institution of Civil Engineers (ICE). The chapter is formatted according publisher guidelines.

Protein aggregation in aqueous polyvinyl alcohol solutions

*Laura E. Hanzly[1], Barbara L. DeButts[2], Danielle Shell[3], and Justin R. Barone[1,2,4]**
[1]Biological Systems Engineering, [2]Macromolecules Innovation Institute,
[3]Interdisciplinary Science and Engineering Program, [4]Center for Soft Matter and Biological Physics
Virginia Tech
Blacksburg, VA 24061

Abstract

Proteins that were previously self-assembled into β-sheet containing structures in aqueous solution are now incubated in aqueous polyvinyl alcohol (PVA) solutions of varying PVA molecular weight and therefore viscosity. Fourier transform infrared (FTIR) spectroscopy shows that self-assembly is driven by protein-protein hydrophobic interactions that correspond to the formation of a β-sheet nanostructure, which is what previous results show happens in purely aqueous solution. Unlike in aqueous solution, self-assembly kinetics are retarded by a factor that is directly related to the PVA solution viscosity. Examination of dried solutions over time with scanning electron microscopy (SEM) shows the formation of "spikes" that organize radially into "pompons". The pompons appear, maximize in number, then disappear with time. Higher viscosity solutions allow for a longer window to see the pompons before disappearance. FTIR spectroscopy and Thioflavin-T staining suggest the spikes are β-sheet containing protein structures. Thermal analysis shows that the aggregated protein structures restrict PVA molecular motion as demonstrated by an increase in its glass transition temperature and increase in PVA crystallinity. The results show that self-assembling proteins in polymer solutions could be an interesting way to form biobased nanocomposites.

*author to whom correspondence should be addressed: jbarone@vt.edu

Keywords
protein aggregation, β-sheet, polyvinyl alcohol, nanocomposites

Introduction

Nanocomposites are nanometer-sized fillers dispersed in polymers.[1] A popular nanofiller is nanoclay, which is composed of anisotropic nanoparticles that are 1-3 nm thick and $>10^4$ nm wide.[2] The nanoclay offers unique increases in mechanical and barrier properties at very low concentration.[3] Typical nanofiller dimensions are such that there is a lot of surface area. So, even at low concentration, the filler comes into contact with a lot of polymer molecules and significantly disrupts the native polymer conformation. This creates a synergy between the nanofiller and the polymer in a typical nanocomposite resulting in the large property increases. But, the huge surface area also creates a lot of surface forces between the particles, even if they are only weak van der Waals forces, but they are summed up many times. Therefore, typical nanofillers prefer to remain agglomerated rather than separate. This makes nanofillers very difficult to separate and disperse into polymers using typical polymer processing equipment.[4, 5]

Processing aids and unusual processing techniques have been developed to separate the nanofillers but have proven to be too expensive to use commercially.[6] One solution has been *in situ* polymerization: dispersing nanofillers in a solution of monomers then polymerizing the monomers into the full polymer to form the nanocomposite. This can only be done with a limited number of polymers and is generally not adaptable to large scale production.[7-9] In contrast, micron-sized fillers in macro-composites do not have as much surface area and are easy to disperse into polymers on typical polymer processing equipment. Micron-sized fillers do not significantly modify the original polymer conformation and only affect the polymer molecules closest to the filler (usually in the "transcrystalline region" if the polymer is semi-crystalline). Therefore, the filler and

polymer remain almost entirely as distinct phases and the properties of the composite are easy to predict from some simple model like a rule of mixtures.[10] However, macro-composites do not approach the property increases achievable with nanocomposites. While the huge advantages of nanocomposites have been reported many times for 20 years, their large volume practical application has not been realized.

It is possible to self-assemble protein molecules into rigid nanostructures called β-sheets.[11, 12] To form the β-sheet, protein molecules are hydrolyzed and/or denatured and straightened so that the main chain carbonyl on one amino acid can hydrogen bond to the main chain secondary amine on another amino acid where the protein inter-chain distance is ~0.47 nm.[13-15] In aqueous solution, hydrophobic groups on amino acid side chains are brought together to thermodynamically induce β-sheet formation.[16-19] In some cases, the β-sheets can elongate and stack to form nanometer-sized fibrils and larger fibrillar structures.[20-22] Theoretical predictions of self-assembled protein nanostructures where inter-chain interactions are through hydrogen bonding yield moduli of E=10-20 GPa.[11] Most experimental results approach these values showing protein nanostructure formation to be a highly evolved process.[23-26] Thus there is substantial interest in using protein nanostructures as reinforcements in polymer composites and previous results show that the reinforcement effect can be significant.[27-34]

We have previously studied the self-assembly of trypsin hydrolyzed wheat gluten (THWG) proteins in aqueous solution. Trypsin hydrolysis of wheat gluten results in protein fragments with molecular weights mostly below 10,000 g/mol.[35, 36] The changes in inter-molecular interactions, morphology, and mechanical properties of the self-assembled protein nanostructures were characterized.[16, 22, 37-40] We then hypothesized that

THWG proteins could be self-assembled in polymers to make environmentally-friendly, biobased, and potentially fully biodegradable nanocomposites through "*in situ*" nanofiller formation. This could be a solution to forming nanocomposites without using extreme compounding conditions and would thus be effective and overall much "greener". We have recently shown the reinforcement of rubber while also increasing the biobased content by compounding THWG proteins into synthetic polyisoprene rubber.[41] In another incarnation, we self-assembled THWG proteins in aqueous polyvinyl alcohol (PVA) solutions and characterized the mechanical and thermal properties after molding and modulus increases of 89-240% were realized.[42] In this work, we again self-assemble THWG proteins in aqueous PVA solutions but examine the inter-molecular interactions, kinetics, morphology, and thermal property changes during and after self-assembly in detail.

Experimental Section

Materials

Trypsin hydrolyzed wheat gluten (THWG) was prepared by dispersing 20 g of wheat gluten (MP Biomedicals, LLC, Solon, OH) in 800 ml of pure water (25 mg/ml of protein) and hydrolyzing with trypsin (Type I from bovine pancreas, Sigma-Aldrich, St. Louis, MO) at a 1:67 enzyme to substrate ratio (wt:wt). The solution was maintained at 37°C and pH 8 with 1 M NaOH for 72 hours under constant stirring to hydrolyze the protein. The hydrolysis process and characteristics of the resulting hydrolysate have been reported previously.[35-37] The THWG solution was then equally distributed into 3 flasks each containing 25 mg/ml of polyvinyl alcohol (PVA) in pure water to form 50:50 wt:wt

THWG:PVA. 89% hydrolyzed PVA (Sigma-Aldrich, St. Louis, MO) of weight average molecular weight (M_w) 31,000 g/mol (Mowiol 4-88, 31k), 67,000 g/mol (Mowiol 8-88, 67k), and 130,000 g/mol (Mowiol 18-88, 130k) were used. These solutions were incubated at 37°C for 34 days while keeping pH at 8 using 1 M NaOH. PVA controls without protein were incubated under the same solution conditions.

Methods

Fourier Transform-Infrared (FTIR) Spectroscopy. Attenuated total reflectance (ATR) FTIR spectra of the incubating aqueous solutions were recorded every 24 hours on a Thermo Nicolet 6700 FTIR spectrometer (Thermo Fisher Scientific Inc., Waltham, MA) with a 45° ZnSe crystal trough. The aqueous solvent was subtracted from the acquired spectrum to reveal the THWG:PVA spectrum.[39, 43, 44] Three spectra were obtained at each point in time and averages and standard deviations were reported. OMNIC v8.1 software was used to collect and analyze spectra.

Scanning Electron Microscopy (SEM). During the 34-day incubation period, 10 μl of each solution was pipetted onto freshly cleaved mica every 4 days, with the first sample taken right after mixing and equilibrating pH and temperature. Dried samples were mounted on aluminum SEM stubs and coated with a 5 nm layer of iridium. Scanning electron micrographs were acquired using a LEO 1550 field-emission SEM (Zeiss, Peabody, MA) with a 4-6 mm working distance, 5 kV accelerating voltage, and an In-lens SE-detector.

Calculation of "Pompon" Protein Aggregate Density and Diameter. The number of "pompons" in a given area was counted based on SEM images of dried samples at various

time points. Due to the size of the dried samples, multiple SEM images were taken for one sample at any given time point. Pompon number per unit area (um^2) from each image was calculated and then averaged together in order to get the mean and standard deviation of the number of pompons per um^2 for each sample at a given time point. Average pompon diameter was calculated from the measurement of at least 12 pompons (n=12) for each sample at any given time point. If not enough pompons were present, average pompon diameter was not reported for that time point.

Confocal Microscopy and Thioflavin-T Staining. A cryomicrotome was used to cut 6 μm thick cross sections of THWG:31k g/mol PVA. Sample cross sections were mounted on glass slides and stained. Sections were stained with a 1% solution of Thioflavin-T in 90% ethanol and subsequently gently rinsed with 90% ethanol. All confocal microscopy images were taken using an Axio Observer Z1 inverted microscope. For fluorescent images, a GFP filter was used.

Differential Scanning Calorimetry (DSC). DSC analysis was performed on a TA Instruments Q2000 DSC (New Castle, DE). 7.4-7.9 mg samples were placed in TA TZero aluminum pans, covered, and crimped shut. All samples were run in a nitrogen atmosphere at a flow rate of 50 ml/min. A first heat scan was performed from -10ºC to 210ºC at 10ºC/min. The sample was then cooled at 60ºC/min to -10ºC. A second heat scan was performed from -10ºC to 250ºC at 10ºC/min. The thermal transitions were ascertained from the second heating cycle using Universal Analysis software (TA Instruments). The percent crystallinity of the PVA phase (X) was computed using:

$$X = \frac{\Delta H_f}{m_{PVA}\Delta H_f^{\circ}} \quad (1)$$

where ΔH_f is the experimental heat of fusion, m_{PVA} is the mass fraction of PVA in the composite, and ΔH_f°=150 J/g is the theoretical heat of fusion of 100% crystalline PVA.[45,46]

Thermogravimetric Analysis (TGA). TGA was completed on a TA Instruments SDT Q600 (New Castle, DE). 7.5 mg samples were heated at 10ºC/min from room temperature to 600ºC in a nitrogen atmosphere. Nitrogen flow rate was 100 ml/min. Weight loss versus temperature as well as the first derivative of weight loss with temperature (dTGA) versus temperature data were reported.

Viscosity Measurements of PVA Solutions. Apparent viscosity measurements were taken using a DHR3 rheometer (TA Instruments, New Castle, DE) at 37ºC. A concentric cylinder geometry with a cup (radius 15mm) and DIN Rotor (radius 14mm) of height 42mm was used. PVA control solutions were stirred for 24 hours prior to taking measurements in order to ensure the PVA was fully dissolved. Viscosity measurements were obtained by performing a shear rate sweep from 1 to 130 s^{-1}. Lower shear rates did not generate enough shear stress to be accurately read by the force transducer of the rheometer. PVA control solutions exhibited Newtonian behavior with viscosity independent of shear rate over the applied shear rate range (Figure S1).

Results and Discussion

Using FTIR spectroscopy, it has been found that THWG protein self-assembly kinetics are well described by comparing the ratio of the symmetric CH_3 deformation, δ_s, at 1365 cm^{-1} to the asymmetric CH_3 deformation, δ_{as} at 1410 cm^{-1}.[39] PVA only contains 2 CH_3 groups per molecule, which appear at the end of each molecule, and so the strong $\delta(_{CH3})$ absorbances originate in proteins. At the molecular level, the ratio $\delta_s(CH_3)/\delta_{as}(CH_3)$

describes the level of hydrophobic interactions of CH_3 side groups on alanine (A), isoleucine (I), leucine (L), and valine (V) amino acids, which are the thermodynamic driving force for self-assembly in the polar aqueous environment. As THWG self-assembles over time, the ratio of $\delta_s(CH_3)$ to $\delta_{as}(CH_3)$ increases as CH_3 side groups on amino acids pack together. Compared to self-assembly in pure water, protein self-assembly as defined by $\delta_s(CH_3)/\delta_{as}(CH_3)$ is slowed and stunted when placed in aqueous PVA solutions but the inter-molecular interactions in aqueous PVA are similar to those that occur in a purely aqueous environment (Figure 1a). In this study, three different weight average molecular weight (M_w) PVAs are used. The extent of protein self-assembly is dependent on PVA M_w, where there is a higher level of aggregation in lower M_w PVA solutions at a given time. The ratio $\delta_s(CH_3)/\delta_{as}(CH_3)$ correlates with the secondary structure change of the protein, which is quantified by the FTIR ratio 1620 cm^{-1}/1272 cm^{-1} (Figure S2).[37-39] The 1620 cm^{-1} contribution to the Amide I absorbance represents the high density β-sheets typical of self-assembled protein nanostructures.[39] The ν(CO) absorbance at 1272 cm^{-1} appears only in the PVA spectrum and represents the stretching of a carbon-oxygen bond in a polyalcohol.[47, 48] Therefore, the ratio 1620 cm^{-1}/1272 cm^{-1} represents the amount of protein β-sheets relative to the PVA phase.

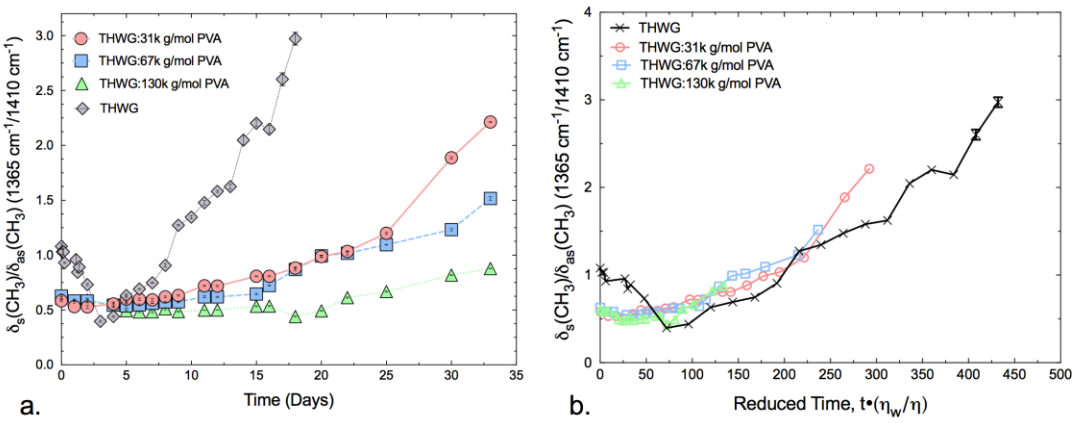

Figure 1. Comparing the ratio of the symmetric CH_3 deformation to the asymmetric CH_3 deformation, $\delta_s(CH_3)/\delta_{as}(CH_3)$, quantifies the level of hydrophobic interactions during self-assembly (a). Included for comparison is the pure THWG protein in aqueous solution.[37] Comparison of hydrophobic interactions versus reduced time, in hours, shows kinetics of self-assembly are similar across solutions (b).

The viscosity of the self-assembly medium is dependent on the PVA M_w, with higher M_w producing higher viscosity solutions and compare well with other reports of PVA solution viscosity (Table1 and Figure S1).[49] At a given self-assembly time point, there is a larger extent of hydrophobic interactions in lower viscosity solutions because it is easier for protein molecules to find each other and assemble. The self-assembly time is converted to "reduced time" by multiplying it by the ratio η_w/η, where η_w is the viscosity of water at 37°C (0.00069 Pa*s) and η is the viscosity of the PVA solution. In reduced time space, the self-assembly kinetics are all similar (Figure 1b) showing that the hydrophobic interactions dominate the self-assembly in any medium and that the kinetics are simply retarded by the respective viscosity of the solution.

Table 1. Viscosities of PVA control solutions.

Control PVA Solution (2.5 wt%)	**Apparent Viscosity (η x 10^3 Pa*s)**
31k g/mol	1.87 ± 0.10
67k g/mol	2.31 ± 0.08
130k g/mol	4.08 ± 0.10

No discernible regular features are observed in PVA control samples incubated and dried under the same conditions as those with protein and PVA (Figure 2). The typical structure observed in protein-PVA mixtures is an anisotropic "spike" of 200-350 nm width (Figure 3). The spike width is largely invariant with time and is not affected by the difference in viscosity between PVA solutions (Figure S3). The spikes eventually arrange into "pompons" where one spike end aggregates closely with the others and then the spikes extend outward radially (Figures 4, 5c, 5d, and S4). Pompons of 5-12 μm diameter (Figure 6) are composed of spikes of 200-350 nm width. Previous work has shown that THWG β-sheet nanostructures exhibit a green fluorescence when stained with Thioflavin-T.[37] The spikes in the pompons stain positive for Thioflavin-T, suggesting that the spikes are protein and have an underlying β-sheet structure, also corroborating the FTIR results (Figure 5b). The PVA control samples are also kept at pH 8 using the same NaOH buffer. However, the PVA controls require higher amounts of NaOH to keep them at a pH 8 so have more salt than the PVA:THWG composites. It seems unlikely that the spikes are salt or they would appear in the PVA controls.

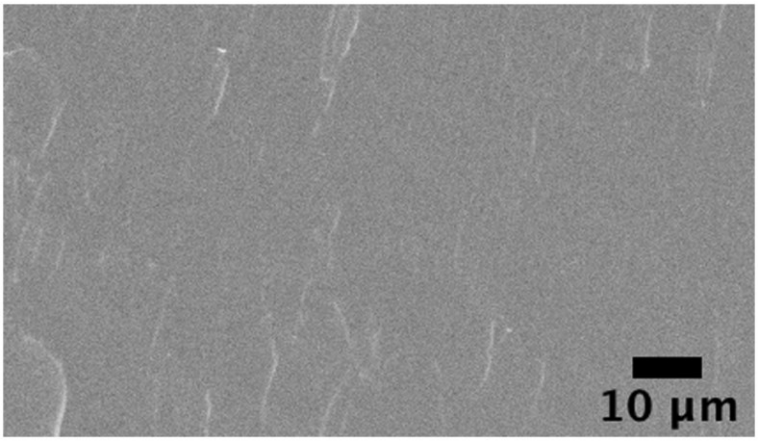

Figure 2. Pure PVA controls show no regular surface features when incubated under the same conditions as the samples with protein.

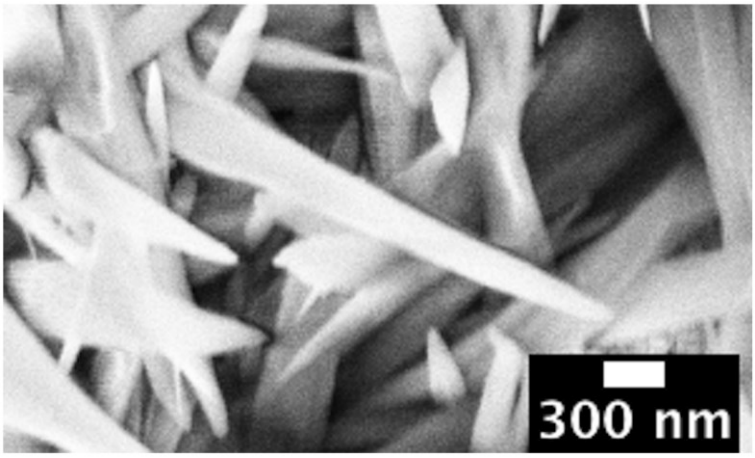

Figure 3. An example of a self-assembled protein "spike". The spike widths remain 200-350 nm throughout the process.

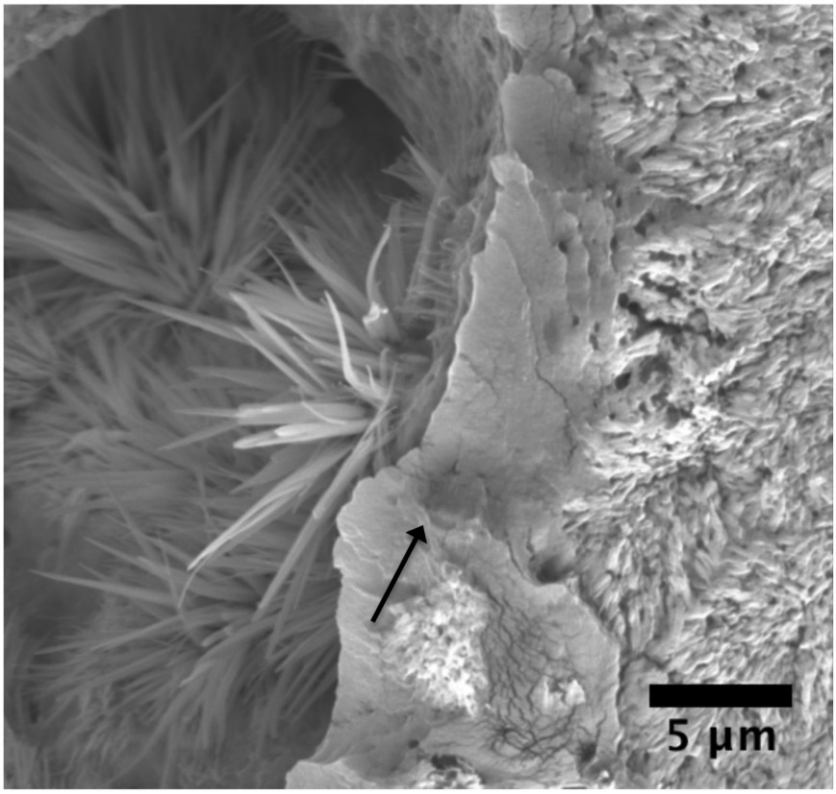

Figure 4. SEM image of spikes and unassembled surrounding material. The black arrow points to a region that appears different than the material in the rest of the image and could point to unassembled protein or PVA.

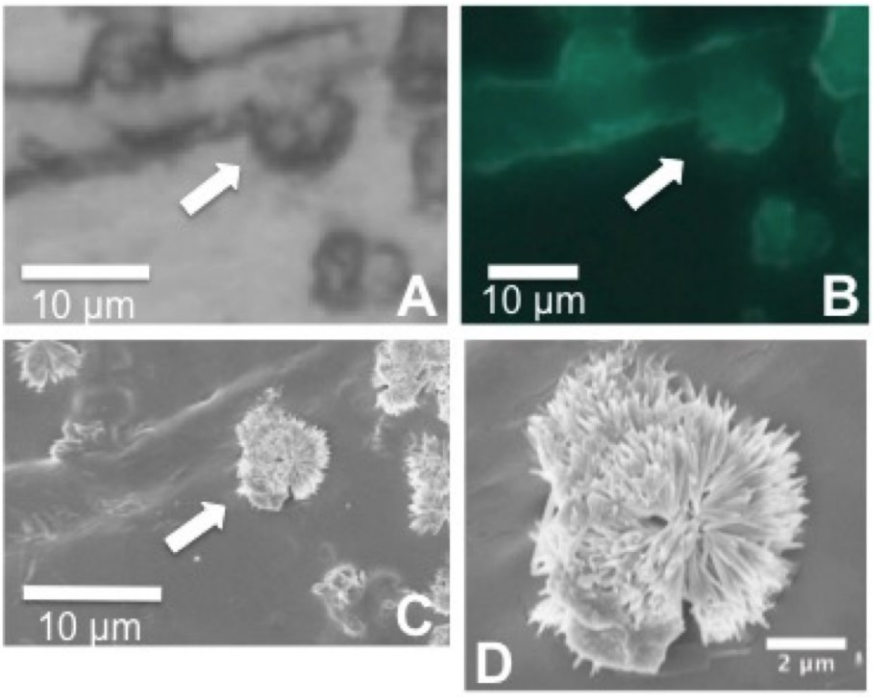

Figure 5. Images of agglomeration of protein spikes in THWG:31k g/mol PVA composites. (a) Brightfield microscopy of a 6 µm thick cross section of THWG:31k g/mol PVA composite. (b) Protein aggregates fluoresce green when stained with Thioflavin-T, indicative of β-sheet structure. (c) SEM of the same portion of cross section observed in (a) and (b). Fully spherical spiked agglomerates or "pompons" are present as well as partially formed pompons. (d) Close up of pompon. Arrows in images indicate location of pompon observed in (d).

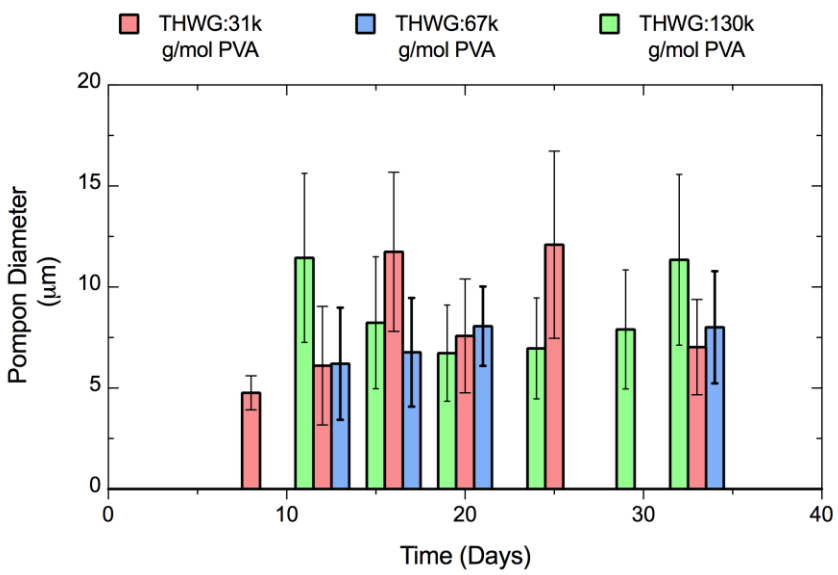

Figure 6. Pompon diameter does not vary with time or solution viscosity.

The appearance of spikes and pompons is dependent on the surrounding medium viscosity. For THWG:31k g/mol PVA, individual spikes appear at day 4 and pompons at day 8. For THWG:67k g/mol PVA and THWG:130k g/mol PVA, individual spikes appear at day 8 and pompons at day 12. The pompon number density (# pompons/μm^2) increases then slowly decreases with time (Figure 7). Just like the first appearance of spikes and pompons is dependent on the surrounding medium viscosity, so is the time at which pompon number density maximizes. The time, t, for the first observation of spikes, pompons, and the maximum pompon number density are listed in Table 2. Also listed in Table 2 are the corresponding hydrophobic interaction values as measured by the δ_s/δ_{as} ratio from FTIR spectroscopy (Figure 1). While the time to observe each phenomenon is different and depends on the solution viscosity, the level of hydrophobic interactions are surprisingly constant for each event. For example, the average hydrophobic interaction required for spikes to first appear is δ_s/δ_{as}=0.55 and for pompon number density to maximize is δ_s/δ_{as}=0.66. This implies that about 20% (0.66/0.55) more hydrophobic

interactions are required for spikes to maximize their agglomeration into pompons before disappearing. There is some scatter in the THWG:130k g/mol PVA data and the δ_s/δ_{as} values given in parentheses are the values if a smooth curve is assumed through the data points. Although spikes appear early, continued hydrophobic interactions as measured by FTIR spectroscopy also play a role in larger scale structure formation beyond the molecular level. In this case, the formation of pompons. Hydrophobic interactions on already formed β-sheet containing amyloid fibrils are also responsible for the further bundling of fibrils into larger structures.[50, 51] From the time of first spike appearance to the time of maximum pompon number density, an observer would have 8, 8, and 17 days in 31k g/mol, 67k g/mol, and 130k g/mol PVA aqueous solutions, respectively, to observe pompons. In pure water, that time would be 1.1 days (Figure 1), a very small window, which may explain why we have previously not observed pompons in our THWG system. Similarly sized and looking Aβ protein spikes that agglomerate into pompons have been observed previously *in vivo* in APP23 transgenic (tg) mice.[52] Those pompons also disappeared over time. We observed pompons in another study and the pompons densified when the THWG:PVA composites were compression molded.[42]

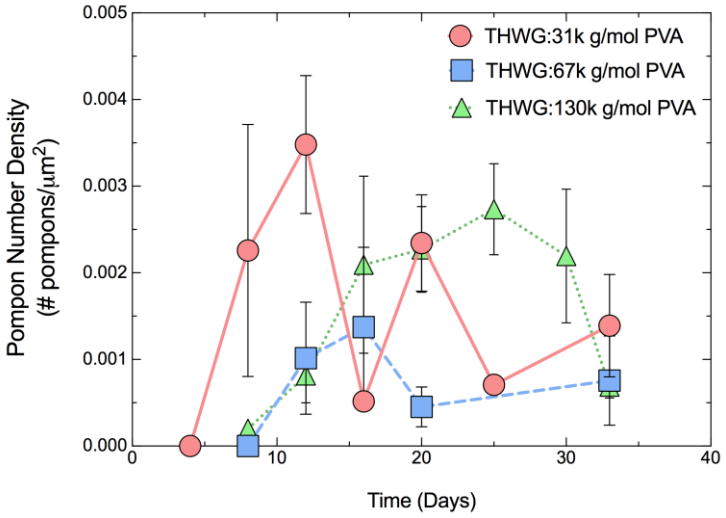

Figure 7. Pompons appear, maximize their number, then slowly disappear with time. The first point in time for each sample indicates the initial observance of spikes (Table 1).

Table 2. Characteristic time points in pompon formation as observed in SEM and FTIR.

	Spike appearance		Pompon appearance		Pompon number density maximum	
Sample	**t (day)**	**δ_s/δ_{as}**	**t (day)**	**δ_s/δ_{as}**	**t (day)**	**δ_s/δ_{as}**
THWG:31k g/mol PVA	4	0.56	8	0.61	12	0.68
THWG:67k g/mol PVA	8	0.58	12	0.63	16	0.69
THWG:130k g/mol PVA	8	0.52	12	0.45 (0.53)	25	0.62 (0.68)

Table 3 lists the glass transition temperature (T_g) and melting (temperature, T_m, and percent crystallinity, X) results from the 2nd heat scan (Figure S5 and S6). T_g changes with the PVA M_w where T_g is highest for the lowest PVA M_w of 31,000 g/mol and trends inversely with the PVA M_w. T_m also shows the same trend. The DSC scans are taken on samples after the full 34-day incubation period. THWG:31k g/mol PVA composites have a higher number of spikes and pompons than the other composites at this time (Figure 7). The results suggest that more protein aggregates (spikes, pompons) in the lower M_w PVA

composites restrict amorphous PVA molecular motion resulting in a higher T_g. The higher PVA M_w composites have less protein aggregates to restrict PVA molecular motion resulting in a lower T_g and all of the composites have a higher T_g than the PVA control showing that the presence of the protein restricts PVA molecular motion overall. In the presence of aggregated protein molecules, higher M_w PVA results in smaller PVA crystals (lower T_m) but more of them (higher X) and the T_m and X are higher in all of the composites compared to the PVA control (Figure 8).

Table 3. Thermal properties of PVA control and THWG:PVA composites.

Sample	T_g (°C)	T_g depth, d (W/g)	T_m (°C)	X (%)
67k PVA control	64.5	0.090	187.9	18.1
THWG:31k g/mol PVA	72.3	0.045	205.9	24.7
THWG:67k g/mol PVA	71.4	0.051	202.1	28.2
THWG:130k g/mol PVA	68.4	0.059	197.3	31.7

The composites are also analyzed with thermogravimetric analysis (TGA) by heating from room temperature to 600°C at 10°C/min (Figure 9). The addition of protein lowers the temperature of the main degradation event but increases the temperature of the final degradation event. This could be because only some of the protein self-assembles. The unassembled protein could be lowering the major degradation event temperature while the self-assembled protein structures stabilize the composites and raise the temperature of the final degradation event. Self-assembled protein β-sheet structures have been shown to be stable to temperature.[53, 54]

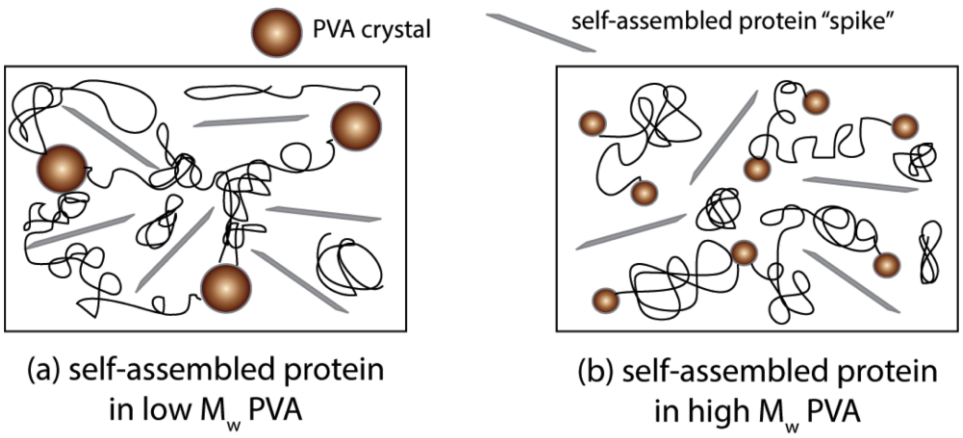

Figure 8. Molecular model based on SEM and DSC results showing possible morphologies for THWG:PVA composites.

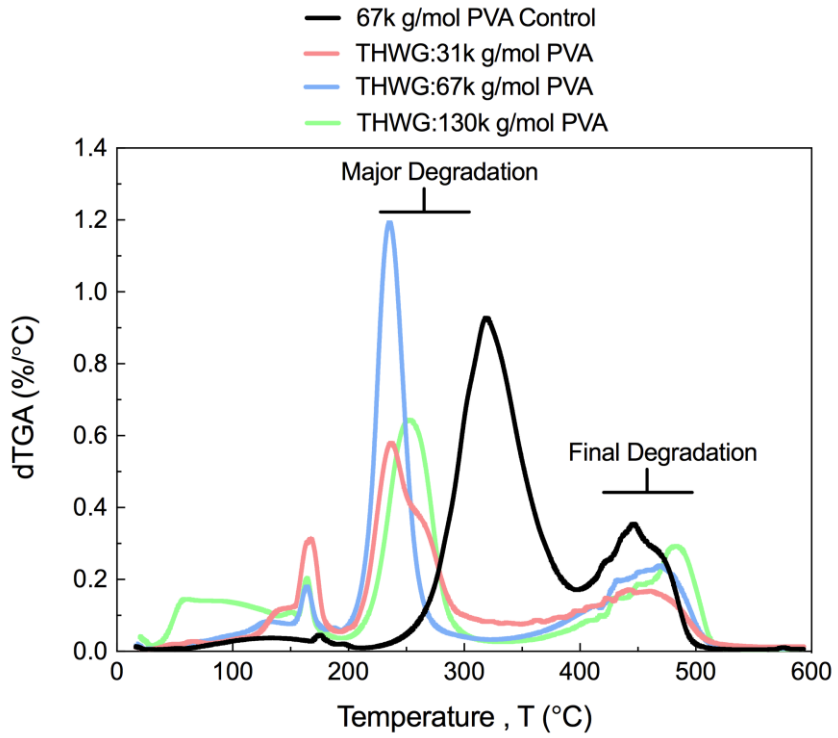

Figure 9. dTGA results for PVA control and THWG:PVA composites.

Conclusions

Proteins can be self-assembled into anisotropic structures in high viscosity polar polymer solutions. The anisotropic structures formed in PVA solutions are spikes, which are differently shaped than the fibrils formed in aqueous solution. At a given time during self-assembly, there is more extensive molecular aggregation in low viscosity solutions but ultimately the self-assembly process in any solution is the same and only changed kinetically by the solution viscosity. Spikes will eventually agglomerate into pompons. The first appearance of spikes and pompons and the observation of the maximum number density of pompons all correlate with the solution viscosity with lower viscosity solutions showing earlier appearance and pompon number maxima. Independent of the solution viscosity and appearance time, the protein in each solution shows constant values of hydrophobic interactions as measured by FTIR spectroscopy, indicating a universal assembly process through protein hydrophobic groups. Hydrophobic groups are not only responsible for protein molecular assembly but larger scale assembly into spikes. Protein aggregates restrict PVA molecular motion resulting in a higher glass transition temperature. The presence of protein also changes PVA crystallinity number and size with higher M_w PVA resulting in more small crystals. Protein aggregates enhance PVA thermal stability but the unassembled protein detracts from it. The results suggest that bio-based, multi-phase nanocomposites could be formed from an aqueous solution containing self-assembling proteins and polymer matrix.

Supporting Information

Viscosity measurements of PVA control solutions for **1,** graph of $\delta_s(CH_3)/\delta_{as}(CH_3)$ ratio versus 1620 cm^{-1}/1272 cm^{-1} for **2**, spike width data over time for **3**, additional micrographs of pompons for **4**, DSC T_g data for **5**, and DSC T_m data for **6**.

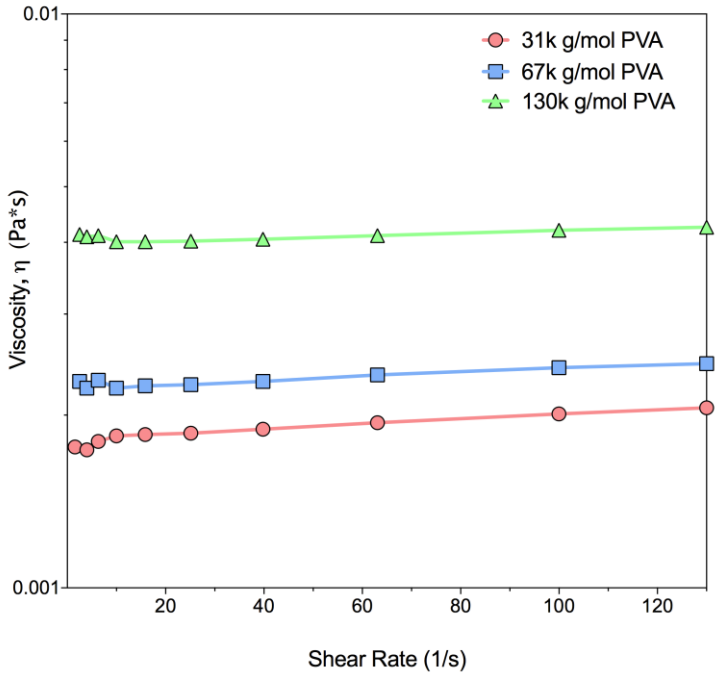

Figure S1. Viscosity measurements with increasing shear rate for each of three different M_W PVA solutions.

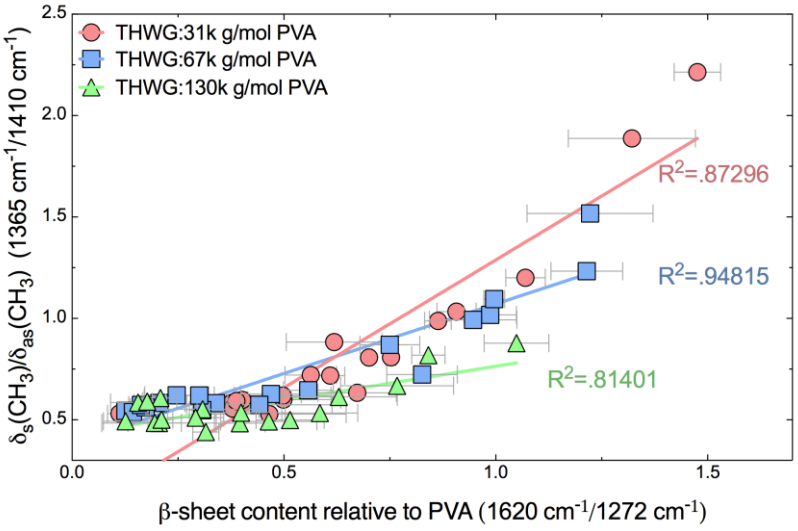

Figure S2. The extent of hydrophobic interactions, $\delta_s(CH_3)/\delta_{as}(CH_3)$, correlates with the amount of protein β-sheets in the THWG:PVA composites.

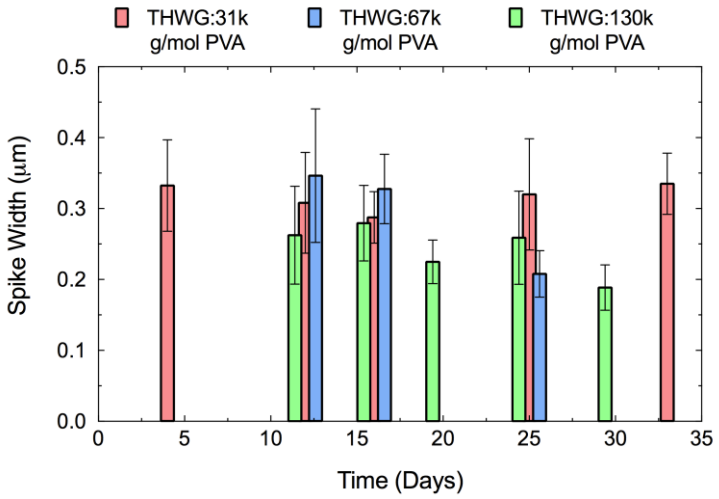

Figure S3. Anisotropic spike width is invariant with self-assembly time and medium viscosity. Sample data is missing from select time points due to lack of available spikes at an appropriate angle to accurately measure spike width.

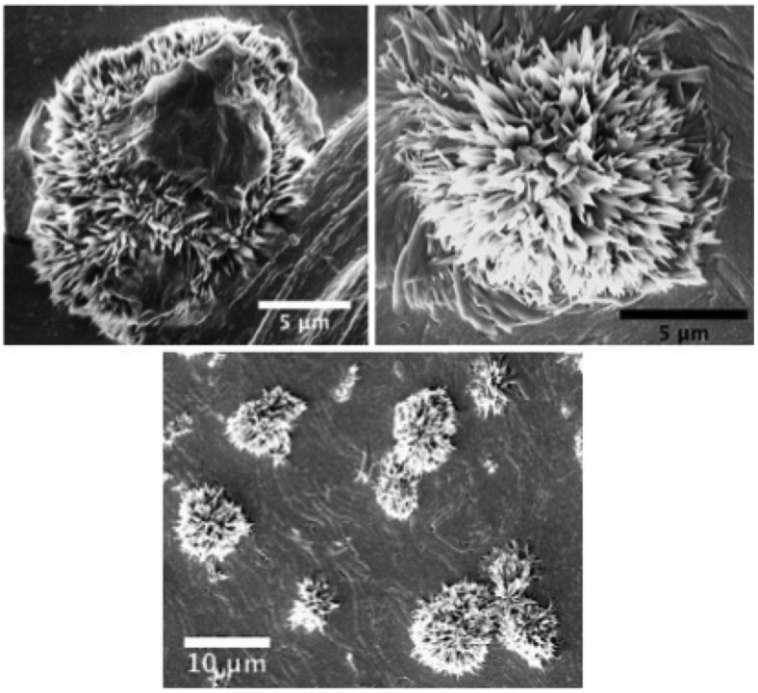

Figure S4. Additional photos of pompons observed in protein-PVA samples.

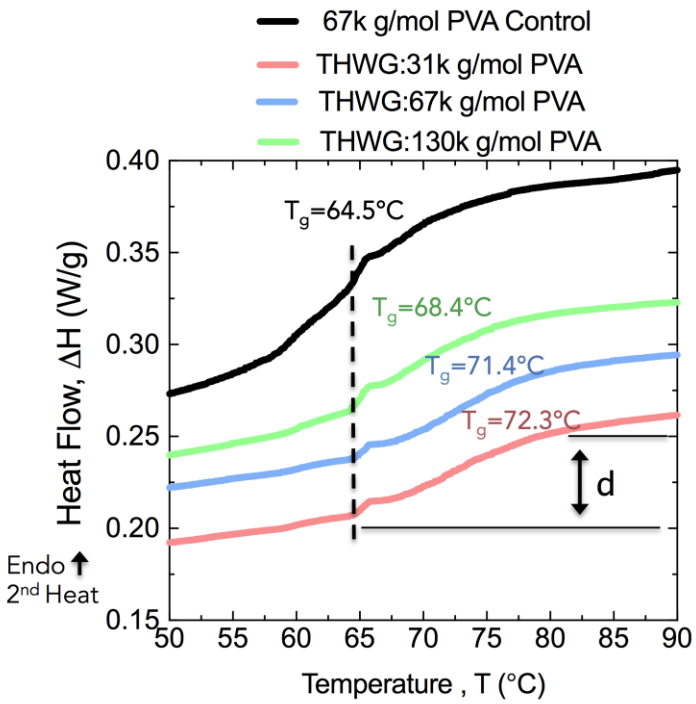

Figure S5. Glass transition temperature (T_g) from second DSC heating scan.

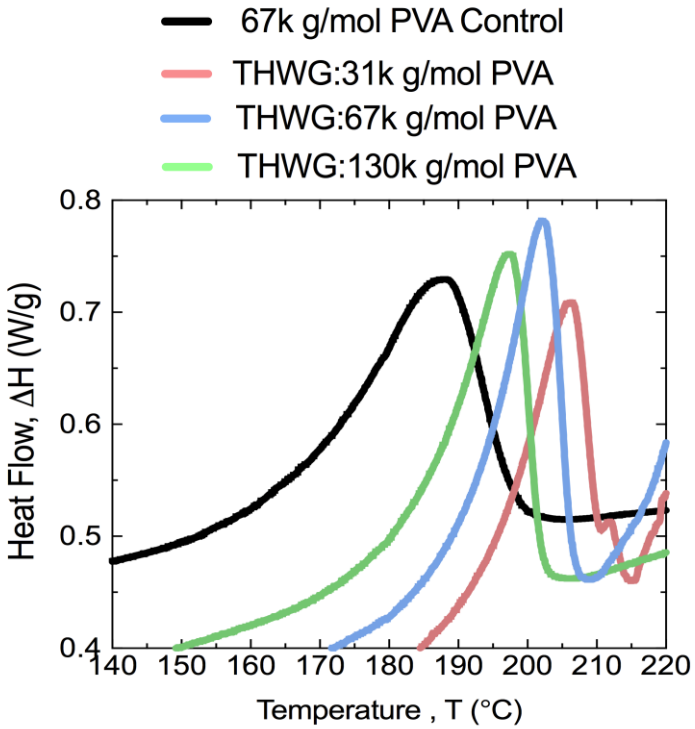

Figure S6. Melting behavior from DSC second heating scan.

Acknowledgments

Generous funding was provided by USDA-2016-67021-25006. Laura Hanzly was supported by a Graduate Teaching Scholarship (GTS) at Virginia Tech.

References

1. Tang, X. Z.; Kumar, P.; Alavi, S.; Sandeep, K. P. Recent Advances in Biopolymers and Biopolymer-Based Nanocomposites for Food Packaging Materials, *Critical Reviews in Food Science and Nutrition*. **2012,** ***52,*** 426-442.
2. Giannelis, E. P. Polymer Layered Silicate Nanocomposites, *Advanced Materials*. **1996,** ***8,*** 29-35.
3. Vaia, R. A.; Giannelis, E. P. Polymer Nanocomposites: Status and Opportunities, *MRS Bulletin*. **2001,** ***26,*** 394-401.
4. Sinha Ray, S.; Okamoto, M. Polymer/layered silicate nanocomposites: a review from preparation to processing, *Progress in Polymer Science*. **2003,** ***28,*** 1539-1641.
5. Pavlidou, S.; Papaspyrides, C. D. A review on polymer–layered silicate nanocomposites, *Progress in Polymer Science*. **2008,** ***33,*** 1119-1198.
6. Podsiadlo, P.; Choi, S.-Y.; Shim, B.; Lee, J.; Cuddihy, M.; Kotov, N. A. Molecularly Engineered Nanocomposites: Layer-by-Layer Assembly of Cellulose Nanocrystals, *Biomacromolecules*. **2005,** ***6,*** 2914-2918.
7. Ou, Y.; Yang, F.; Yu, Z.-Z. A new conception on the toughness of nylon 6/silica nanocomposite prepared via in situ polymerization, *Journal of Polymer Science Part B: Polymer Physics*. **1998,** ***36,*** 789-795.
8. Zeng, C.; Lee, L. J. Poly(methyl methacrylate) and Polystyrene/Clay Nanocomposites Prepared by in-Situ Polymerization, *Macromolecules*. **2001,** ***34,*** 4098-4103.
9. Sun, T.; Garcés, J. M. High-Performance Polypropylene–Clay Nanocomposites by In-situ Polymerization with Metallocene/Clay Catalysts, *Advanced Materials*. **2002,** ***14,*** 128-130.
10. Chawla, K. K. *Composite Materials*, New York: Springer-Verlag, 1987.
11. Knowles, T. P. J.; Buehler, M. J. Nanomechanics of functional and pathological amyloid materials, *Nature Nanotechnology*. **2011,** ***6,*** 469-479.
12. Knowles, T. P. J.; Mezzenga, R. Amyloid Fibrils as Building Blocks for Natural and Artificial Functional Materials, *Adv Mater*. **2016,** DOI 10.1002/adma.201505961**,** n/a-n/a.
13. Makin, O. S.; Sikorski, P.; Serpell, L. C. Diffraction to study protein and peptide assemblies, *Curr Opin Chem Biol*. **2006,** ***10,*** 417-422.
14. Serpell, L. C.; Smith, J. M. Direct visualisation of the β-sheet structure of synthetic Alzheimer's amyloid, *J Mol Biol*. **2000,** ***299,*** 225-231.
15. Sunde, M.; Serpell, L. C.; Bartlam, M.; Fraser, P. E.; Pepys, M. B.; Blake, C. C. F. Common core structure of amyloid fibrils by synchrotron X-ray diffraction, *J Mol Biol*. **1997,** ***273,*** 729-739.
16. Ridgley, D. M.; Claunch, E. C.; Lee, P. W.; Barone, J. R. The role of protein hydrophobicity in conformation change and self-assembly into large amyloid fibers, *Biomacromolecules*. **2014,** ***15,*** 1240-1247.

17. Adamcik, J.; Mezzenga, R. Adjustable twisting periodic pitch of amyloid fibrils, *Soft Matter*. **2011,** ***7,*** 5437-5443.
18. Eisenberg, D.; Weiss, R. M.; Terwilliger, T. C.; Wilcox, W. Hydrophobic moments and protein structure, *Faraday Symposia of the Chemical Society*. **1982,** ***17,*** 109-120.
19. Eisenberg, D.; Wilcox, W.; McLachlan, A. D. Hydrophobicity and amphiphilicity in protein structure, *Journal of Cellular Biochemistry*. **1986,** ***31,*** 11-17.
20. Bolisetty, S.; Adamcik, J.; Mezzenga, R. Snapshots of fibrillation and aggregation kinetics in multistranded amyloid β-lactoglobulin fibrils, *Soft Matter*. **2011,** ***7,*** 493-499.
21. Lara, C. c.; Adamcik, J.; Jordens, S.; Mezzenga, R. General Self-Assembly Mechanism Converting Hydrolyzed Globular Proteins Into Giant Multistranded Amyloid Ribbons, *Biomacromolecules*. **2011,** ***12,*** 1868-1875.
22. Ridgley, D. M.; Barone, J. R. Evolution of the amyloid fiber over multiple length scales, *ACS Nano*. **2013,** ***7,*** 1006-1015.
23. Adamcik, J.; Berquand, A.; Mezzenga, R. Single-step direct measurement of amyloid fibrils stiffness by peak force quantitative nanomechanical atomic force microscopy, *Appl Phys Lett*. **2011,** ***98,*** 193701.
24. Adamcik, J.; Lara, C.; Usov, I., et al. Measurement of intrinsic properties of amyloid fibrils by the peak force QNM method, *Nanoscale*. **2012,** ***4,*** 4426-4429.
25. Paul, T. J.; Hoffmann, Z.; Wang, C., et al. Structural and Mechanical Properties of Amyloid Beta Fibrils: A Combined Experimental and Theoretical Approach, *The Journal of Physical Chemistry Letters*. **2016,** ***7,*** 2758-2764.
26. Sasaki, N.; Saitoh, Y.; Sharma, R. K.; Furusawa, K. Determination of the elastic modulus of β-lactoglobulin amyloid fibrils by measuring the Debye-Waller factor, *Int J Biol Macromol*. **2016,** ***92,*** 240-245.
27. Oppenheim, T.; Knowles, T. P. J.; Lacour, S. P.; Welland, M. E. Fabrication and characterisation of protein fibril–elastomer composites, *Acta Biomaterialia*. **2010,** ***6,*** 1337-1341.
28. Knowles, T.; Lacour, S.; Welland, M. *Polymer composite and method for its manufacture.* 2010.
29. Welland, M.; Knowles, T.; Oppenheim, T. *Materials based on filamentous peptide or protein-based structures.* 2010.
30. Byrne, N.; Hameed, N.; Werzer, O.; Guo, Q. The preparation of novel nanofilled polymer composites using poly(l-lactic acid) and protein fibers, *European Polymer Journal*. **2011,** ***47,*** 1279-1283.
31. Rao, S. P.; Meade, S. J.; Healy, J. P., et al. Amyloid fibrils as functionalizable components of nanocomposite materials, *Biotechnology Progress*. **2012,** ***28,*** 248-256.
32. Ling, S.; Li, C.; Adamcik, J.; Shao, Z.; Chen, X.; Mezzenga, R. Modulating Materials by Orthogonally Oriented β-Strands: Composites of Amyloid and Silk Fibroin Fibrils, *Adv Mater*. **2014,** ***26,*** 4569-4574.
33. Li, C.; Bolisetty, S.; Mezzenga, R. Hybrid Nanocomposites of Gold Single-Crystal Platelets and Amyloid Fibrils with Tunable Fluorescence, Conductivity, and Sensing Properties, *Adv Mater*. **2013,** ***25,*** 3694-3700.
34. Li, C.; Born, A.-K.; Schweizer, T.; Zenobi-Wong, M.; Cerruti, M.; Mezzenga, R. Amyloid-Hydroxyapatite Bone Biomimetic Composites, *Adv Mater*. **2014,** ***26,*** 3207-3212.

35. Athamneh, A.; Barone, J. R. Enzyme-mediated self-assembly of highly ordered structures from disordered proteins, *Smart Mater Struct*. **2009, *18,*** 104024 (104028pp).
36. Tuck, C. S.; Latham, A.; Lee, P. W.; Barone, J. R. Wheat gluten plasticized with its own hydrolysate, *J Polym Environ*. **2014, *22,*** 430-438.
37. Ridgley, D. M.; Ebanks, K. C.; Barone, J. R. Peptide mixtures can self-assemble into large amyloid fibers of varying size and morphology, *Biomacromolecules*. **2011, *12,*** 3770-3779.
38. Ridgley, D. M.; Claunch, E. C.; Barone, J. R. The effect of processing on large, self-assembled amyloid fibers, *Soft Matter*. **2012, *8,*** 10298-10306.
39. Ridgley, D. M.; Claunch, E. C.; Barone, J. R. Characterization of large amyloid fibers and tapes with Fourier transform infrared (FT-IR) and Raman spectroscopy, *Appl Spectrosc*. **2013, *67,*** 1417-1426.
40. Hall, D. M.; Bruss, I. R.; Barone, J. R.; Grason, G. M. Morphology selection via geometric frustration in chiral filament bundles, *Nat Mater*. **2016, *15,*** 727-732.
41. DeButts, B. L.; Hanzly, L. E.; Barone, J. R. Protein-polyisoprene rubber composites, *Journal of Applied Polymer Science*. **2018, *135,*** 46026-n/a.
42. DeButts, B. L.; Spivey, C. R.; Barone, J. R. Wheat Gluten Aggregates as a Reinforcement for Poly(vinyl alcohol) Films, *ACS Sustainable Chemistry & Engineering*. **2018, *6,*** 2422-2430.
43. Goormaghtigh, E.; Cabiaux, V.; Ruysschaert, J.-M. Secondary structure and dosage of soluble and membrane proteins by attenuated total reflection Fourier-transform infrared spectroscopy on hydrated films, *European Journal of Biochemistry*. **1990, *193,*** 409-420.
44. Vendantham, G.; Sparks, H. G.; Sane, S. U.; Tzannis, S.; Przybycien, T. M. A holistic approach for protein secondary structure estimation from infrared spectra in H_2O solutions, *Analytical Biochemistry*. **2000, *285,*** 33-49.
45. Finch, C. A. *Polyvinyl alcohol; properties and applications*, London: John Wiley & Sons, 1973.
46. Lu, J.; Wang, T.; Drzal, L. T. Preparation and properties of microfibrillated cellulose polyvinyl alcohol composite materials, *Composites Part A: Applied Science and Manufacturing*. **2008, *39,*** 738-746.
47. Pereira Jr., V. A.; de Arruda, I. N. Q.; Stefani, R. Active chitosan/PVA films with anthocyanins from *Brassica oleraceae* (red cabbage) as time-temperature indicators for application in intelligent food packaging, *Food Hydrocolloids*. **2015, *43,*** 180-188.
48. Li, M.; Zhou, H.-h.; Li, T.; Li, C.-y.; Xia, Z.-y.; Duan, Y. Y. Polyurethane/poly(vinyl alcohol) hydrogel coating improves the cytocompatibility of neural electrodes, *Neural Regeneration Research*. **2015, *10,*** 2048-2053.
49. Fried, J. R. *Polymer Science and Technology*, Englewood Cliffs: Prentice Hall PTR, 1995.
50. Jung, J.-M.; Mezzenga, R. Liquid Crystalline Phase Behavior of Protein Fibers in Water: Experiments versus Theory, *Langmuir*. **2010, *26,*** 504-514.
51. Adamcik, J.; Jung, J.-M.; Flakowski, J.; De Los Rios, P.; Dietler, G.; Mezzenga, R. Understanding amyloid aggregation by statistical analysis of atomic force microscopy images, *Nature Nanotechnology*. **2010, *5,*** 423-428.

52. Meyer, E. P.; Ulmann-Schuler, A.; Staufenbiel, M.; Krucker, T. Altered morphology and 3D architecture of brain vasculature in a mouse model for Alzheimer's disease, *Proc Natl Acad Sci USA*. **2008,** ***105,*** 3587-3592.
53. Safar, J.; Roller, P. P.; Gajdusek, D. C.; Gibbs, C. J. Thermal stability and conformational transitions of scrapie amyloid (prion) protein correlate with infectivity, *Protein Sci*. **1993,** ***2,*** 2206-2216.
54. Meersman, F.; Dobson, C. M. Probing the pressure–temperature stability of amyloid fibrils provides new insights into their molecular properties, *Biochim Biophys Acta*. **2006,** ***1764,*** 452-460.

CHAPTER 3: GELATIN HYDROGEL BILAYER ACTUATORS

Hanzly, L.E., Kristofferson, K.A., and Barone, J.R., (2019). Gelatin Hydrogel Bilayer Actuators.

Gelatin hydrogel bilayer actuators

*Laura E. Hanzly[1], Kristofer A. Kristofferson[2],and Justin R. Barone[1,3,4]**
[1]Biological Systems Engineering, [2]NSF REU: Food-Energy-Water Systems, Macromolecules Innovation Institute, [3]Macromolecules Innovation Institue, [4]Center for Soft Matter and Biological Physics
Virginia Tech
Blacksburg, VA 24061

Abstract

Gelatin can be crosslinked to various degrees with glutaraldehyde (GTA) and swollen with water to form a hydrogel. As gelatin crosslink density increases, gel stiffness increases and swelling in water decreases with crosslink density saturating at about 0.01 moles of GTA. Forming gelatin hydrogel bilayers with layers of differing crosslink density results in a gelatin actuator that bends towards the layer of higher crosslink density when swollen in water. The extent of bilayer bending is dependent upon the difference between the volume swelling ratio of the layers, which is directly determined by the crosslink density difference. When the gelatin bilayers are close in swell ratio or when the swell ratio is significantly different no bending occurs. The highest bending is found when the higher crosslinked passive layer swells to about 60% of the lower crosslinked active layer. Filling the active layer with pre-gelatinized starch increases the bilayer curvature but it returns to its original shape after hydrolyzing the starch with α-amylase. The results show that simple gelatin bilayers can serve as cyclic actuators when stimulated with water or sugar and enzyme.

*author to whom correspondence should be addressed: jbarone@vt.edu

Introduction

Gelatin is the hydrolysis product of animal collagen. It is valued for its simplicity, economy, and ability to be used in a variety of applications particularly in the biomedical and food industries.[1, 2] Thus, it is safe to use and biocompatible. Gelatin can be formed into physically-crosslinked hydrogels in hot water so it is very easy to process. Depending on how it is processed, the native helical collagen structure can be regained or the gel can remain amorphous so its properties can be varied in a straightforward manner.[3] Physically-crosslinked gelatin typically has low modulus and stability. The modulus and stability can be increased by introducing chemical crosslinks or intermolecular covalent bonds similar to a vulcanized rubber. There are many ways to chemically crosslink gelatin including using diisocyanates, cyanamide, UV light, and the enzyme transglutaminase.[4-7] Aldehydes will readily react with the lysine or hydroxylysine amino acids on collagen so this is a simple way to chemically crosslink gelatin.[8-10] The mechanism is not completely understood but involves a nucleophilic addition onto available amine groups, of which the ε-amine on lysine side groups in proteins is considered the preferred site.[11, 12]

A hydrogel is special because it can be swollen to a high extent with water such that the resulting material is overwhelmingly water (i.e., > 90%) while the swollen but not completely dissolved polymer remains in the minority. This creates a soft material that still has mechanical integrity and is biocompatible. The equilibrium volume swelling ratio, Q, is defined as the ratio of the total swollen volume attainable (polymer + water solvent), V_T, to the dry polymer volume, V_p:

$$Q = \frac{V_T}{V_p} = \frac{1}{v_p} \qquad (1)$$

where ν_p is the polymer volume fraction in the water swollen hydrogel.[13] Hydrogels attain high values of Q, i.e., it could be 10 or higher. This large volume change suggests that hydrogels would make good "soft machines" when introduced to water, something akin to a gas-filled piston-cylinder device that is capable of performing work when the gas is heated and expanded.[14] Traditionally, the term robot has been associated with rigid machines designed to perform a specific and precise task based on some form of user input. However, the need for machines that are flexible and adaptable to changes in environment has led to the emerging field of soft robotics.[15-17] Soft robots are deformable so they can conform to objects based on external stimuli and fill spaces. Not only are soft robots spatially conformable compared to rigid-bodied robots, they also offer the advantage of being safer in terms of human interaction due to their compliant nature. Preparing soft robots from hydrogels would also make them biocompatible and similar to the working parts inside humans and animals like tendon, ligament, and muscle, which are all protein hydrogels.[18]

One of the key elements for the continued development of soft robotics is the design and fabrication of novel sensors and soft actuators.[15, 19] Soft actuators constructed from natural or synthetic elastomeric materials are sensitive to environmental fluctuations in pH, solvent, heat, humidity, electric field, light, etc., resulting in the conversion of chemical and physical energy into mechanical work.[20] Current examples of materials used for soft actuation include shape-memory polymers[21], ionic liquids and polymers[22-24], various forms of hydrogels[25], electroactive polymers[23], and carbon nanotubes[26]. The implementation of these materials into actuator designs often requires expensive and tedious processing such as lithography, multi-material 3D printing, and shape deposition manufacturing (SDM).[17]

Finding a material that is inexpensive as well as easily manipulated and mass-producible for soft actuation is a current challenge for commercial applications of soft robots.

Here we present a gelatin hydrogel soft actuator that bends in response to swelling in water or addition of starch into the actuator and hydrolysis of small sugars out of it. Gelatin is of particular interest in designing soft actuators as it can easily be manipulated, poured into molds, and crosslinked to various degrees resulting in a variety of shapes and mechanical properties when swollen in water. The gelatin bilayers are then swelled with soluble starch and more bending is realized. Hydrolysis of the starch with the enzyme α-amylase returns the gelatin bilayer to its original shape.

Materials and Methods

Rheology. To determine the crosslinking and modulus limits of the gelatin system, gelatin gels were created by dissolving 20 wt% gelatin from bovine skin (Type B, 225 Bloom, G9382 from Sigma Aldrich, St. Louis, MO) in deionized water at 40°C and then pouring 35 ml of the gelatin solution into a glass petri dish (9 cm in diameter) and allowing it to dry for 24 hours. The dried gelatin was then cut into 2.5 cm diameter discs. The 2.5 cm gelatin discs were then crosslinked using glutaraldehyde (GTA) solutions (340855 from Sigma Aldrich, St. Louis, MO) at concentrations varying from 0.01% to 50% GTA (w/v). For each GTA concentration, three discs were crosslinked per 100 ml of GTA solution in petri dishes. Samples were crosslinked for 24 hours and then washed several times with deionized water. Oscillatory shear experiments were performed using 25 mm parallel plates on a DHR3 rheometer (TA Instruments, New Castle, DE). First, strain sweeps were performed to find the linear viscoelastic region. It was determined that an applied strain of 0.1% would be in the linear viscoelastic region for all crosslink densities. Frequency

sweeps were performed on fully hydrated gelatin control layers as a function of GTA concentration from 0.1 to 100 rad/s at 0.1% strain. The gap height between the plates varied based on swollen sample thickness. Three samples at each crosslinking condition were tested and the elastic (storage) modulus, G', was reported as average ± standard error.

Gelatin Bilayers. The hydrogel bilayer design is based on naturally-occurring hydrogel systems and their mimics that bend when swollen with water (Figure 1).[27-34] The initial rheology and swelling results were used as guidance to design the bilayers so that the volume swelling ratio varied between the layers. Again, a 20 wt% gelatin mixture was obtained by dissolving gelatin in deionized water at 40°C. The first layer of the bilayer system was made by pouring 5 ml of the 20 wt% gelatin mixture into a 5.79 cm diameter circular silicone mold (Figure S1, "Bilayer Design"). The gelatin layer was allowed to solidify for 10 minutes before being cut into a smaller 4.4 cm diameter circle using a round metal cutter. The 4.4 cm gelatin circles were then crosslinked in various concentrations of aqueous GTA solution for 30 minutes. The crosslinked gelatin layer was then placed directly on top of 5 ml of freshly poured gelatin in the previously described silicone mold. The gelatin layers were allowed to dry together for 10 minutes before being cut into a smaller 4.4 cm diameter bilayer circle. The gelatin bilayer was then crosslinked with a desired concentration of aqueous GTA solution for 30 minutes. The first layer always had the higher crosslink density, i.e., used a higher concentration GTA solution, and bilayers were referenced as, for example, "2/0.2", which meant a bilayer of 2% GTA in one layer (higher crosslink density passive layer) which was then crosslinked at 0.2% GTA along with the second layer (lower crosslink density active layer). The "passive" and "active" notation and definition was the same used in another study on swellable hydrogel

bilayers.[27] The end result was a circular gelatin bilayer consisting of layers that differed in the amount of crosslinking based on exposure to differing GTA concentrations (Table S1). Controls were created for each individual layer of the bilayer samples in order to measure the volume swelling ratio (Figure S1, "Control Layer Design"). The bilayer cure time was empirically determined to be long enough to get significant curing in the layer placed second but not significantly cure the first layer, which was why the cure time was shorter than for the rheology experiments and the first layer was always subjected to a higher GTA concentration solution.

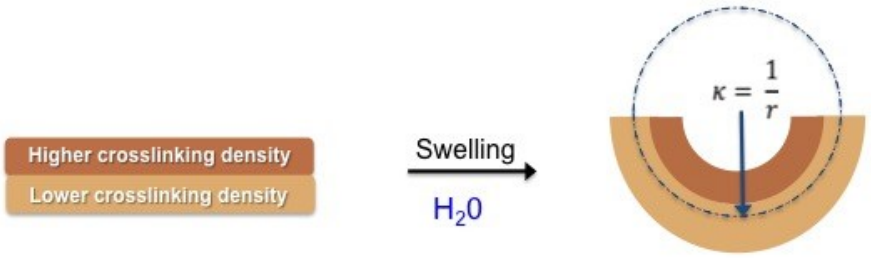

Figure 1. Gelatin bilayer actuating mechanism. Differences in crosslinking cause unequal volume swelling between layers resulting in bilayer bending towards the higher crosslinked side. The higher crosslinked side is the "passive" layer and the lower crosslinked side is the "active" layer in the bilayer.

Swelling Experiments. All gelatin control layers and rheology samples were swollen in deionized water for 48 hours at a room temperature of 25°C after which their fully hydrated, swollen weights, w_w, were recorded. Samples were then allowed to dry at room temperature for another 48 hours before their dry weights, w_d, were recorded. The average volume swelling ratio, Q, and its standard error were calculated from a sample size of 4 for each control layer by:

$$Q = \frac{w_w \rho_{gel}}{w_d \rho_T} \qquad (2)$$

where ρ_{gel}=1.34 g/cm^3 is the density of gelatin[35]. ρ_T is the total density of the water swollen gelatin and can be determined using:

$$\rho_T = \frac{1}{\left[\left(\frac{1}{\rho_{gel}} * \frac{w_d}{w_w}\right) + \frac{1}{\rho_w}\left(1 - \frac{w_d}{w_w}\right)\right]} \quad (3)$$

where ρ_w=0.997 g/cm^3 is the density of water at 25°C, w_d/w_w is the mass fraction of gelatin polymer in the swollen sample and $1-w_w/w_d$ is the mass fraction of water in the swollen sample.

Curvature and Thickness. Gelatin bilayers were allowed to swell in deionized water for 48 hours. Special attention was given to ensure samples had enough space to swell/bend with no obstruction. After 48 hours, bilayers were immediately photographed after being removed from the water. Fiji[36] software was used to measure the radius of curvature, r, of the bilayers (Figure 1) and individual layer thickness of bilayers and control samples. Average curvature, κ=1/r, was then calculated from 4 replicates of each bilayer formulation and was reported along with the standard error. Single layer controls were also swollen and checked for bending but none was observed.

Starch Addition and Hydrolysis. Pre-gelatinized starch was purchased from Barry Farm (Wapakoneta, Ohio). Pre-gelatinized starch was water soluble at room temperature. In order to incorporate starch into the active layer of gelatin bilayers, 20% gelatin solutions were prepared in the same manner as above. Starch was then slowly added and mixed into the active layer gelatin solutions before the entire mixture was poured into molds. Starch was added in at 30 and 50 wt% of the gelatin weight used in the active layer. Bilayers were then constructed and crosslinked as previously described, with the passive layer containing only gelatin and the active layer containing a mixture of starch and gelatin. Starch-gelatin

bilayers were allowed to swell for 48 hours before measuring curvature. α-amylase from *Bacillus licheniformis* (A4551, Sigma Aldrich, St. Louis, MO) was used to digest starch from the bilayers. For each α-amylase treatment, 20 mg of α-amylase was added to 200 ml of de-ionized water. A single bilayer was then placed in the α-amylase solution and allowed to digest for 24 hours. Solutions were placed on a shaker at low speed to ensure the enzyme remained well mixed. Changes in weight and curvature were recorded for 4 replicates and were reported as averages ± standard error.

Results and Discussion

Crosslinked gelatin storage modulus, G', increases and volume swell ratio, Q, decreases with increasing GTA concentration (Figure 2). G' and Q should be inversely proportional because higher crosslink density means less swelling and more stiffness according to the Flory-Rehner theory.[37] Both properties saturate at a GTA concentration of about 0.01 moles (1% GTA solution) for the samples cured for 24 hours (higher concentration data not shown but remains constant). Gelatin obtained from animal skin is largely composed of Type I collagen.[38] α-2 Type I bovine collagen (UniProt P02465, 129,064 g/mol) and α-1 Type I bovine collagen (UniProt P02453, 138,939 g/mol) have 50/1364 and 57/1463 lysine (K) amino acids relative to the total number of amino acids, respectively. Assuming an average molecular weight of 134,001 g/mol and each gelatin disk weighs 0.751 g and 3 disks are crosslinked per 100 ml of GTA solution then there are 1.68×10^{-5} moles of gelatin placed in each 100 ml GTA solution (this assumes the full collagen protein and not the hydrolysis product). Assuming an average lysine content of 54 per protein molecule then there are 9.07×10^{-4} moles of lysine available to be crosslinked by GTA, which is 11 times lower than the GTA saturation point of 0.01 moles.

This suggests that GTA polymerizes and/or crosslinks other protein groups such as α-amines in the peptide bond or other nucleophilic amino acid side groups such as arginine and histidine.[11, 12] Glutaraldehyde has also been shown to crosslink hydroxyl groups but at much different conditions than used here.[39] Regardless of the actual mechanism, GTA offers a way to achieve great variation in crosslink density, which affects the final volume swelling and therefore modulus of the gelatin layer.

As a check on the consistency of the gelatin-water system, the Flory-Rehner theory is used to find the Flory-Huggins interaction parameter, χ, from the data in Figure 2 to compare it to literature values. Using G' and Q from Figure 2 and a crosslink functionality of f=4, Flory-Huggins interaction parameter values of χ=0.55-0.60 at Q=6.0-3.7 are found, which are in very good agreement with other reports of χ for gelatin/water over similar water content.[40, 41]

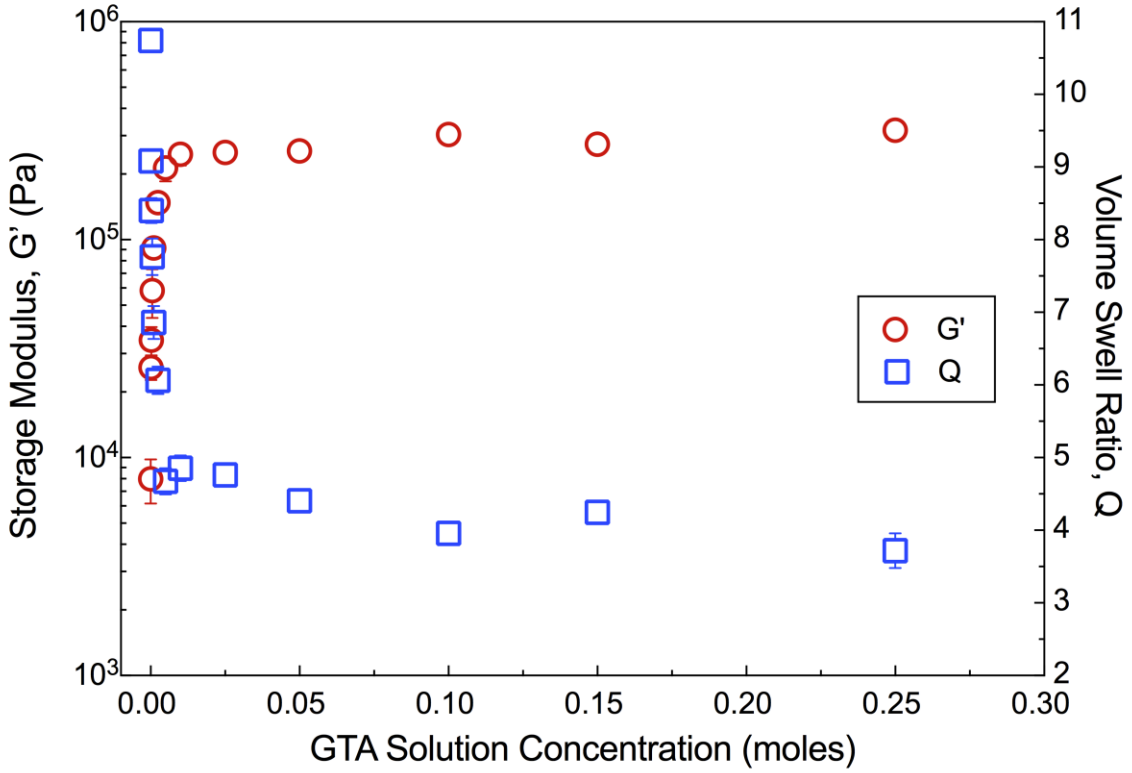

Figure 2. Gelatin storage modulus, G', and volume swell ratio, Q, as a function of GTA solution concentration used for crosslinking.

Gelatin bilayers of different crosslink density were prepared by varying the GTA content in each layer so as to realize a volume swelling difference. Swelling the bilayers in water is a rather slow process and is limited by the diffusion of water into the polymeric structure (Figure 3). Bilayers are allowed to swell in deionized water for 48 hours prior to measuring the curvature but full curvature is observed within 24 hours.

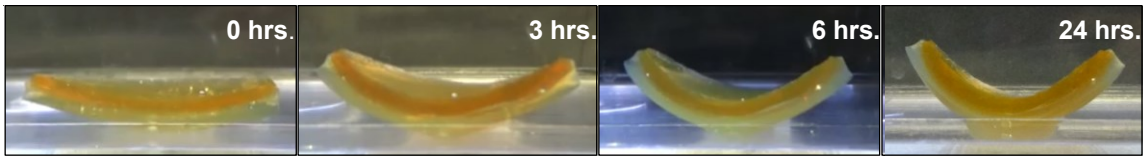

Figure 3. Gelatin bilayer bending over time. Bilayers are allowed to swell for a total period of 48 hours. Bending between 24-48 hrs. is not significant enough to include a picture. GTA "1/0.05" bilayer shown.

The measured curvature of each bilayer is plotted against the ratio of the volume swelling of the passive layer, Q_p, to the active layer, Q_a (Figure 4). Here "passive" is defined as the higher crosslinked, less swelled layer while "active" is defined as the less crosslinked, more swelled layer. The volume swelling ratios are found experimentally from the individual layers. Bilayer bending has clear limitations based on crosslinking differences between layers. Bilayer curvature is nonexistent or extremely low in bilayers with $Q_p/Q_a \rightarrow 1$. When each layer is similarly swollen, there is no impetus for curvature, which occurs for lightly crosslinked layers, i.e., when the molecular weight between crosslinks, M_c, is quite large. Since Q is directly related to the layer modulus, G' (or M_c) according to the Flory-Rehner theory there is no significant mismatch in modulus between the layers. For bilayers with $Q_p/Q_a \sim 0.35$ there is also limited bending. In this region, the active layer swells much more than the passive layer. The less swollen passive layer is too stiff and resists the bending imposed by the highly swollen active layer. Maximum bilayer curvature occurs at $Q_p/Q_a \sim 0.6$ when the passive layer is not too stiff to resist the bending of the more swollen active layer. The data in Figure 4 is similar to that predicted by a theoretical model where no bending occurs when $Q_p/Q_a \rightarrow 0$ and $Q_p/Q_a \rightarrow 1$, for the reasons given above, with a maximum in between.[27] The theoretical model has the layer thickness and modulus ratios as separate parameters but here we treat them as one parameter, which is the volume swelling ratio. These results show that curvature, a large-scale continuum mechanical parameter, can be predicted from M_c, a molecular level parameter, through the ratio Q_p/Q_a.

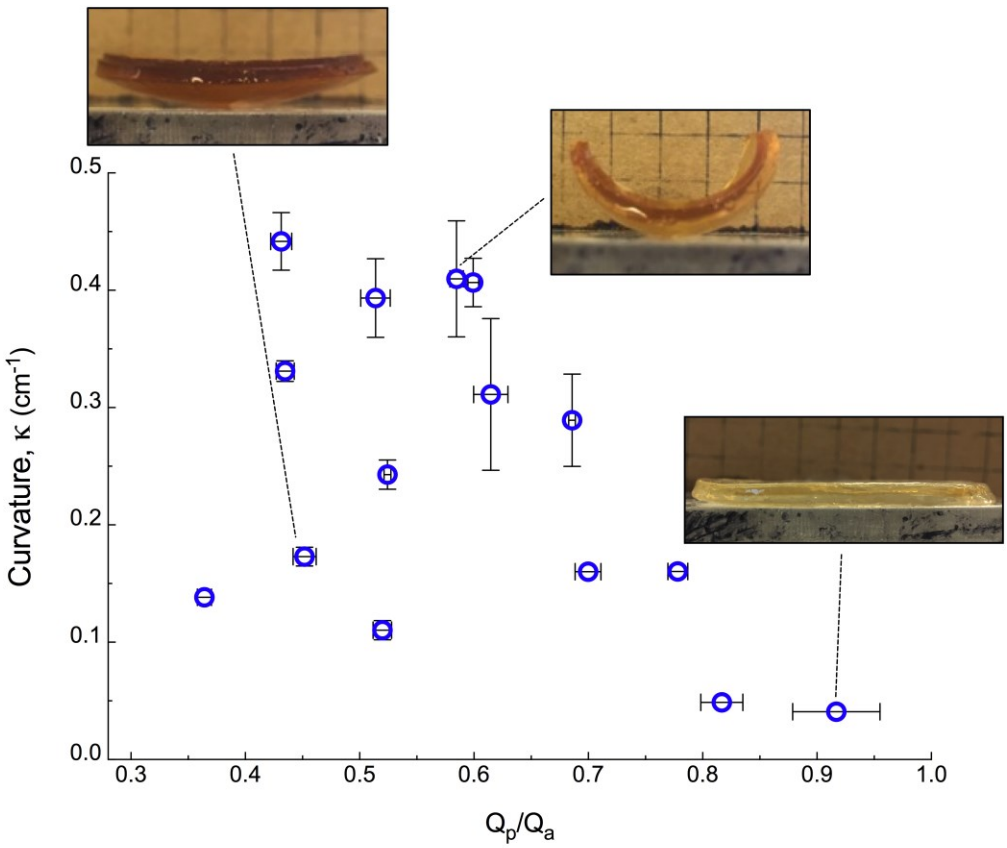

Figure 4. Average curvature for each bilayer. Pictures on graph show actual bending for that particular bilayer. The GTA concentration of each Q_p/Q_a value can be referenced in Table S1.

To cycle a bilayer between the curved and uncurved states, water would have to be diffused into and out of the bilayer. While relatively slow, this would also result in complete or near complete drying of the bilayer. Instead, it was hypothesized that a fully hydrated cyclic system could be made by using soluble or pre-gelatinized starch in the active layer to affect the curvature and then α-amylase enzyme to hydrolyze the starch such that it would diffuse out and return it back to its original state. Thus, a completely wet cyclic actuator could be made that would behave similarly to an actual biological system and work on a simple biochemical reaction. The first bilayer chosen was the 1/0.05 system with $Q_p/Q_a=0.51 \pm 0.03$ (Table S1). This was chosen because it was at the peak of the

curvature graph in Figure 1 with $\kappa=0.39 \pm 0.03$ cm^{-1}. Originally it was hypothesized that the starch would incorporate into the bilayer as part of the polymer fraction, thus increasing ν_p and decreasing Q_a for the active layer, resulting in a flat bilayer that would have been highly curved without the starch because now Q_a would be closer to Q_p. Hydrolyzing the starch and allowing the small molecular weight sugars to diffuse out would return the bilayer back to the curved state. Surprisingly, the addition of pre-gelatinized starch to the active layer of gelatin bilayers results in an increase in curvature with more starch addition resulting in more curvature (Figure 5). This is because incorporation of pre-gelatinized starch increases the volume swelling ratio of the active layer, Q_a, causing an increase in the swelling difference between the active and passive layers and therefore more curvature (Figure 5b). This is confirmed by swelling the individual active layer with starch (Figure S2).

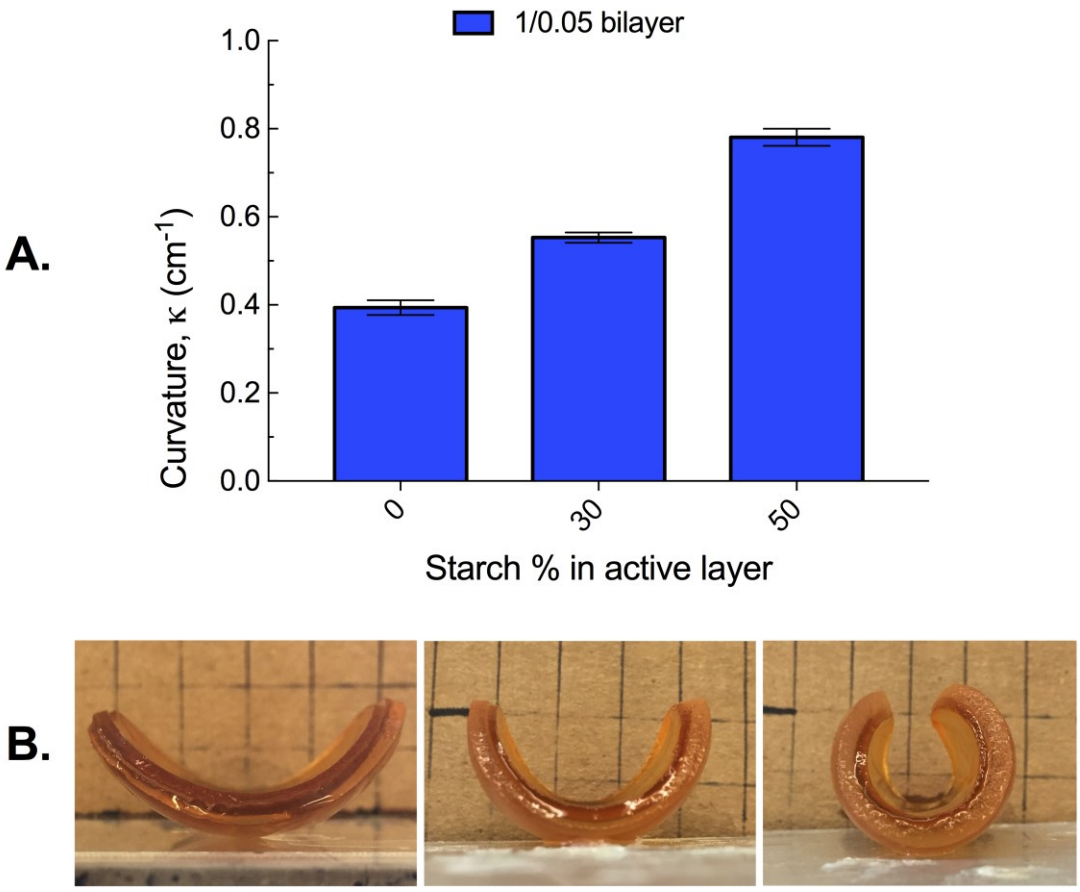

Figure 5. (a) Starch addition to active layer of "1/0.05" gelatin bilayer results in increased curvature. (b) 1/0.05 gelatin bilayer (left), 1/(0.05 +30% starch) bilayer (middle), and (1/0.05 + 50% starch) bilayer (right). The active layer is on the bottom and is more opaque than the passive top layer.

Gelatin bilayers that exhibit no or very minimal bending can be coaxed into bending through the incorporation of starch into the active layer (Figure 6). The "0.125/0.0125" bilayer exhibits no curvature when it is comprised of just gelatin layers (Q_p/Q_a=0.92 ± 0.08, κ=0.04 ± 0.01, Table S1 and Figure 2). The addition of 50% starch into the 0.0125 active layer increases the curvature of the bilayer approximately 10-fold. In order to return the bilayers to the original lower curvature the enzyme α-amylase is used to digest starch from

the starch-gelatin active layer in the bilayers. When treated with α-amylase, starch-gelatin bilayers dramatically decrease in curvature and return to the original flat state (Figure 6).

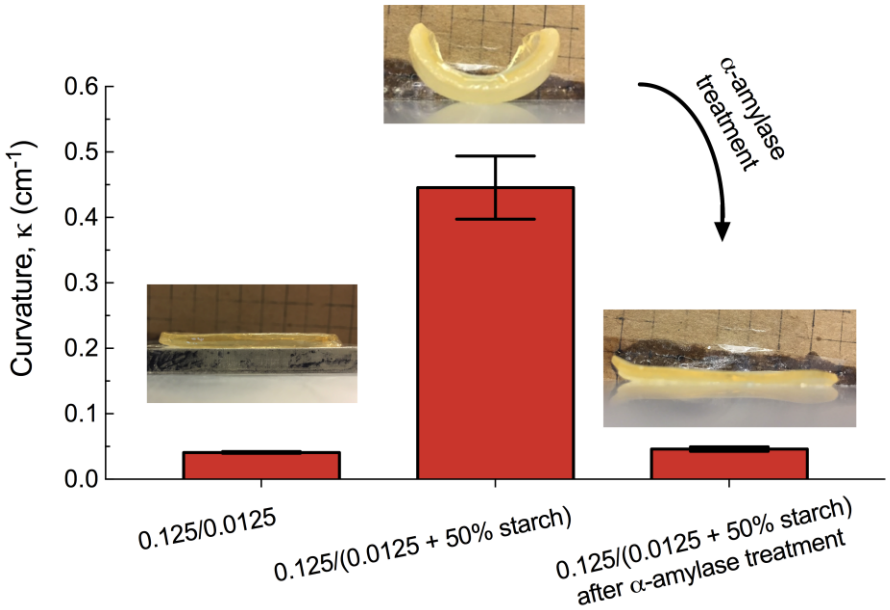

Figure 6. Gelatin bilayers that display no curvature will bend with the incorporation of starch into the active layer. 50% starch is added to the active layer of 0.125/0.0125 bilayers. The starch filled bilayers demonstrate significant bending compared to the 0.125/0.0125 starch-free bilayers. Treating the starch-gelatin bilayers with α-amylase eliminates the increase in curvature caused by starch.

Cyclic actuation, i.e., changing shape in response to a stimulus and then returning to the original shape in response to another stimulus, is crucial for soft actuator design. Starch incorporation yields bilayers with increased curvature in comparison to their gelatin bilayer controls (Figures 5 and 6). Upon α-amylase treatment, the curvature is reduced. This decrease in curvature is accompanied by a significant decrease in weight (Figure 7). This decrease in bilayer weight is the result of starch being digested and leaving the gelatin active layer. The addition of α-amylase to starch-free gelatin bilayers does not decrease the weight, indicating that the α-amylase is only digesting the starch in the starch-filled bilayers (Figure S3). Additionally, starch gelatin bilayers swollen in de-ionized water do

not decrease in weight, so starch is not diffusing out of starch-gelatin matrices on its own (Figure 7 "No α-amylase").

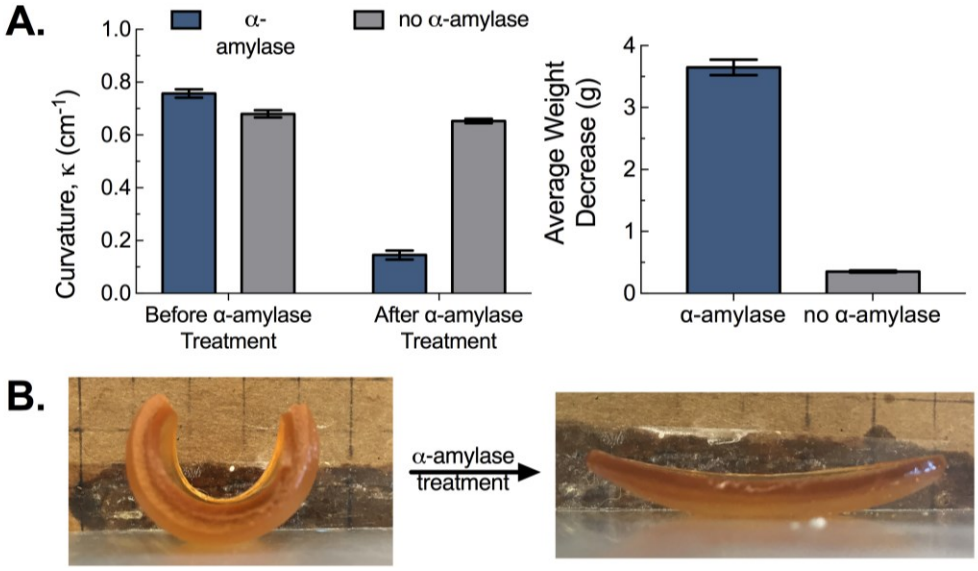

Figure 7. (a) 1/(0.05 + 50% starch) bilayers treated with α-amylase. The presence of α-amylase results in decreased bilayer curvature and weight. "No α-amylase" group consists of 1/(0.05 + 50% starch) bilayers not treated with α-amylase but still swollen in deionized water for the same amount of time as the "α-amylase" group. The "no α-amylase" group does not show a decrease in weight or curvature. (b) Visual of curvature change of 1/(0.05 + 50% starch) bilayer after α-amylase treatment.

The 0.125/0.0125 bilayer starts off at $\kappa=0.04 \pm 0.01$ prior to starch addition. After starch addition, $\kappa=0.45 \pm 0.08$. Upon starch hydrolysis with α-amylase and diffusion of the small sugars out of the gelatin matrix, the curvature decreases to $\kappa=0.05 \pm 0.01$. This indicates a full recovery of the original gelatin bilayer structure after cycle completion. The 1/0.05 bilayer starts off at $\kappa=0.39 \pm 0.03$ cm^{-1}. After starch addition, curvature increases to $\kappa=0.74 \pm 0.02$. Upon starch hydrolysis with α-amylase, curvatures decreases to $\kappa=0.16 \pm 0.02$. Unlike the 0.125/0.0125 layer, the 1/0.05 bilayer does not return to its original curvature after starch hydrolysis. This insinuates hysteresis in the gelatin active

and/or passive layer. The higher active layer volume swell ratio may break part of the original active and/or passive layer network structure and introduce hysteresis in the cycle. It is not uncommon for highly strained networks to break at high volume swelling in solvent so that upon removal of the strain and recovery the network does not return to its original unstrained state.[42] Two challenges remain to continue with subsequent cycles: (1) understand and minimize actuator hysteresis and (2) diffuse starch back into the active layer. The former could be solved by swelling the active layer less and the latter by diffusing starch at a higher temperature, where the gelatin network becomes more mobile and open and the starch diffusion constant increases. The majority of the starch diffusion would be into the more open active layer with starch diffusion into the passive layer retarded by a factor related to its increased crosslink density.

Conclusions

Gelatin hydrogels were formed that behaved as typical solvent swollen gels with elastic moduli that increased and volume swelling that decreased with increased crosslinking. Gelatin bilayers were created where there was a volume swelling mismatch between the less swelled passive layer, Q_p, and the more swelled active layer, Q_a. When $Q_p/Q_a \rightarrow 1$ the layers did not have enough of a volume swelling mismatch to induce bilayer curvature upon swelling. When $Q_p/Q_a \rightarrow 0$ the stiffer passive layer resisted the swelling of the highly swollen active layer and there was no bilayer curvature. At $Q_p/Q_a \sim 0.6$, maximum curvature of $\kappa = 0.40\text{-}0.45$ cm^{-1} was realized. To make a cyclic bilayer system, water would have to be diffused into and out of the bilayer, which would result in a dry bilayer on one part of the cycle. To maintain a hydrated system and realize a cycle, water soluble pre-gelatinized starch was incorporated into the active layer of the bilayer. This resulted in higher active

layer volume swelling and more bilayer curvature. Upon hydrolysis of the starch with α-amylase and diffusion out of the active layer, the bilayer lost its highly curved state and completed the cycle. The simple cyclic system described could be used as an actuator in soft robots. It would also be used as a shape-shifting hydrogel to realize texture in foods upon eating because α-amylase exists in saliva. It could also be used to deliver nutraceuticals, flavor, or drugs upon ingestion.

Acknowledgements

Laura Hanzly was supported by a Graduate Teaching Scholarship (GTS) at Virginia Tech. Kristofer A. Kristofferson performs portions of this research while participating in the NSF- Research Experience for Undergraduates (REU) program "Food-Water-Energy Systems" [Grant NSF-1560240].

Supplementary Information

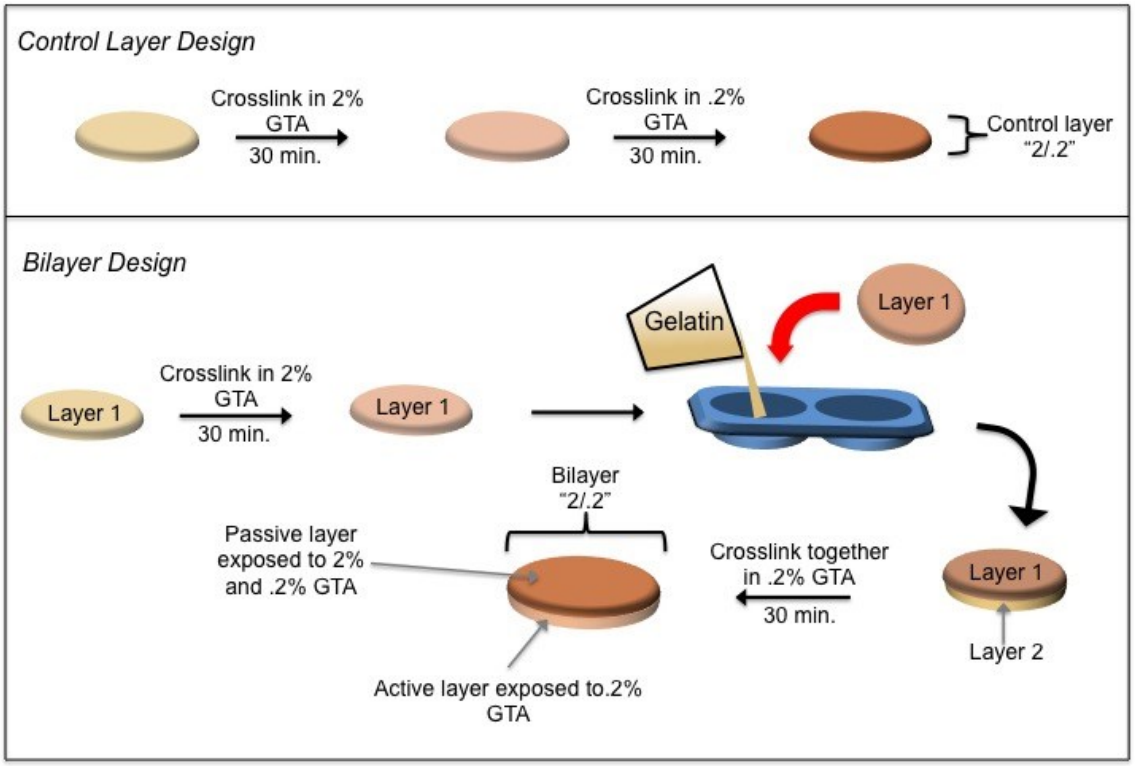

Figure S1. Example of fabrication and nomenclature of gelatin control layer (top) and bilayer (bottom). For the control layer, the name denotes what GTA percentage crosslinked the layer. For example, "2/0.2" indicates that the gelatin layer was first crosslinked with 2% GTA for 30 minutes and then crosslinked with 0.2% GTA for another 30 minutes to form the "2/0.2" control layer (top). Bilayer name indicates the crosslinking of the passive and active layers together. For the bilayer "2/0.2", the passive layer was first crosslinked with 2% GTA and then the active and passive layers were crosslinked together in 0.2% GTA to form a bilayer consisting of a passive layer crosslinked with both 2% and 0.2% GTA and an active layer crosslinked with 0.2% GTA (bottom). Data included in Table S1.

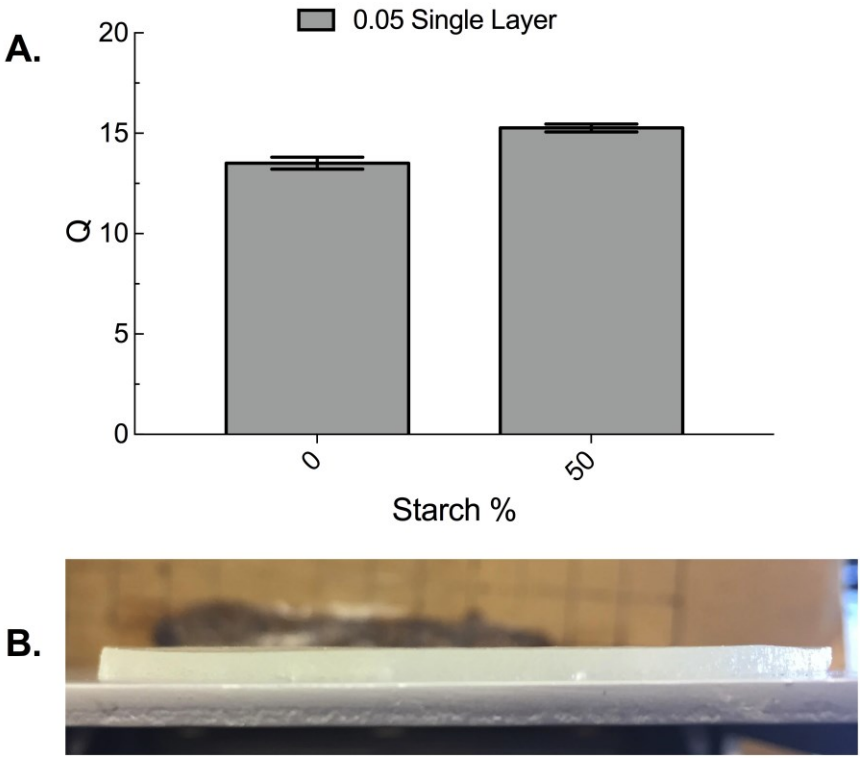

Figure S2. (a) Swelling difference between 0.05 gelatin single layer and (0.05 +50% starch) gelatin single layer. Starch incorporation increases the equilibrium swelling ratio, Q_a, of the active layer. (b) Starch incorporation into single gelatin layers does not result in bending.

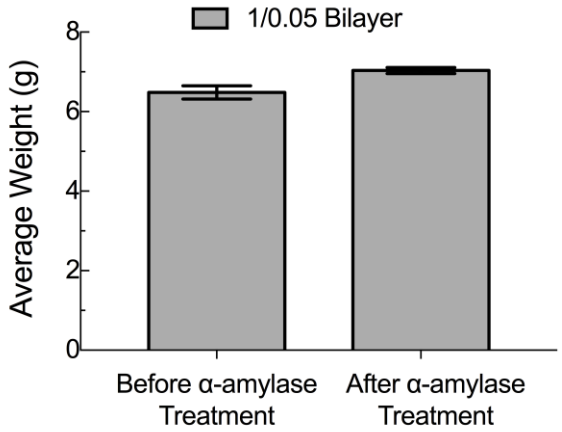

Figure S3. Starch-free 1/0.05 gelatin bilayer subjected to α-amylase treatment. α-amylase does not change the weight of 1/0.05 bilayers indicating the enzyme is not breaking down gelatin.

Table S1. Swelling ratios for individual layers and Q_p/Q_a for bilayers. Control and bilayers are named in accordance with the system described in Figure S1.

Individual Layer	Individual Layer Q	Bilayer	Bilayer Q_p/Q_a
2/0.2	6.0598 ± 0.0144	3/0	0.3643 ± 0.0062
2/0.05	6.1074 ± 0.0273	1/0	0.4349 ± 0.0078
2/0.4	6.1524 ± 0.0453	1/0.00625	0.4314 ± 0.0092
3/0	6.2432 ± 0.0139	2/0.05	0.4519 ± 0.0102
2/0.1	6.2655 ± 0.0279	1/0.05	0.5139 ± 0.0129
1/0.05	6.9458 ± 0.0828	2/0.2	0.5199 ± 0.0082
1/0.1	7.1620 ± 0.0499	2/0.1	0.5244 ± 0.0029
1/0.00625	7.2306 ± 0.0476	0.5/0.025	0.5848 ± 0.0059
1/0	7.4545 ± 0.0451	1/0.1	0.5994 ± 0.0047
0.5/0.1	8.1948 ± 0.0214	0.5/0.05	0.6148 ± 0.0150
0.5/0.05	8.3091 ± 0.0865	0.5/0.1	0.6858 ± 0.0029
0.5/0.025	8.7391 ± 0.0524	2/0.4	0.6998 ± 0.0112
0.4	8.7912 ± 0.1253	0.125/0.025	0.7783 ± 0.0086
0.125/0.025	11.6308 ± 0.0890	0.125/0.00625	0.8168 ± 0.0185
0.2	11.6550 ± 0.1808	0.125/0.0125	0.9169 ± 0.0382
0.1	11.9486 ± 0.0407		
0.125/0.0125	13.2571 ± 0.2786		
0.05	13.5158 ± .2977		
0.125/0.00625	13.6889 ± 0.1356		
0.0125	14.4588 ± 0.5196		
0.025	14.9433 ± 0.1202		
0.00625	16.792 ± 0.3411		
0 (uncrosslinked)	17.1391 ± 0.2908		

References

1. Arvanitoyannis, I. S., *Formation and properties of collagen and gelatin films and coatings*. 2002; p 275-304.
2. Djagny, K. B.; Wang, Z.; Xu, S., Gelatin: A Valuable Protein for Food and Pharmaceutical Industries: Review. *Critical Reviews in Food Science and Nutrition* **2001,** 41, (6), 481-492.
3. Yannas, I. V., Collagen and Gelatin in the Solid State. *Journal of Macromolecular Science, Part C* **1972,** 7, (1), 49-106.
4. Apostolov, A. A.; Boneva, D.; Vassileva, E.; Mark, J. E.; Fakirov, S., Mechanical properties of native and crosslinked gelatins in a bending deformation. *Journal of Applied Polymer Science* **2000,** 76, (14), 2041-2048.
5. Maitra, J.; Shukla, V. K., Cross-linking in hydrogels-a review. *Am. J. Polym. Sci* **2014,** 4, (2), 25-31.
6. Weadock, K.; Olson, R. M.; Silver, F. H., Evaluation of collagen crosslinking techniques. *Biomaterials, medical devices, and artificial organs* **1983,** 11, (4), 293-318.
7. Yung, C. W.; Wu, L. Q.; Tullman, J. A.; Payne, G. F.; Bentley, W. E.; Barbari, T. A., Transglutaminase crosslinked gelatin as a tissue engineering scaffold. *Journal of Biomedical Materials Research Part A* **2007,** 83A, (4), 1039-1046.
8. Cheung, D. T.; Nimni, M. E., Mechanism of Crosslinking of Proteins by Glutaraldehyde II. Reaction with Monomeric and Polymeric Collagen. *Connective Tissue Research* **1982,** 10, (2), 201-216.
9. Farris, S.; Song, J.; Huang, Q., Alternative Reaction Mechanism for the Cross-Linking of Gelatin with Glutaraldehyde. *Journal of Agricultural and Food Chemistry* **2010,** 58, (2), 998-1003.
10. Bigi, A.; Cojazzi, G.; Panzavolta, S.; Rubini, K.; Roveri, N., Mechanical and thermal properties of gelatin films at different degrees of glutaraldehyde crosslinking. *Biomaterials* **2001,** 22, (8), 763-768.
11. Kawahara, J.-i.; Ishikawa, K.; Uchimaru, T.; Takaya, H., Chemical Cross-Linking by Glutaraldehyde between Amino Groups: Its Mechanism and Effects. In *Polymer Modification*, Swift, G.; Carraher, C. E.; Bowman, C. N., Eds. Springer US: Boston, MA, 1997; pp 119-131.
12. Migneault, I.; Dartiguenave, C.; Bertrand, M. J.; Waldron, K. C., Glutaraldehyde: behavior in aqueous solution, reaction with proteins, and application to enzyme crosslinking. *BioTechniques* **2004,** 37, 790-802.
13. Rubinstein, M.; Colby, R. H., *Polymer Physics*. Oxford University Press: Oxford, 2003.
14. Ionov, L., Biomimetic Hydrogel-Based Actuating Systems. *Advanced Functional Materials* **2013,** 23, (36), 4555-4570.
15. Trivedi, D.; Rahn, C. D.; Kier, W. M.; Walker, I. D., Soft robotics: Biological inspiration, state of the art, and future research. *Applied Bionics and Biomechanics* **2008,** 5, (3), 99-117.
16. Majidi, C., Soft robotics: a perspective—current trends and prospects for the future. *Soft Robotics* **2014,** 1, (1), 5-11.
17. Rus, D.; Tolley, M. T., Design, fabrication and control of soft robots. *Nature* **2015,** 521, (7553), 467.

18. Vincent, J. F. V., *Structural biomaterials*. Princeton University Press: 2012.
19. She, Y.; Li, C.; Cleary, J.; Su, H.-J., Design and Fabrication of a Soft Robotic Hand With Embedded Actuators and Sensors. *Journal of Mechanisms and Robotics* **2015,** 7, (2), 021007-021007-9.
20. Asaka, K.; Okuzaki, H., *Soft Actuators: Materials, Modeling, Applications, and Future Perspectives*. Springer: 2014.
21. Behl, M.; Lendlein, A., Shape-memory polymers. *Materials Today* **2007,** 10, (4), 20-28.
22. Jager, E. W. H.; Smela, E.; Inganäs, O., Microfabricating Conjugated Polymer Actuators. *Science* **2000,** 290, (5496), 1540.
23. Armand, M.; Endres, F.; MacFarlane, D. R.; Ohno, H.; Scrosati, B., Ionic-liquid materials for the electrochemical challenges of the future. *Nature Materials* **2009,** 8, 621.
24. Yang, W.; Choi, H.; Choi, S.; Jeon, M.; Lee, S.-Y., Carbon nanotube–graphene composite for ionic polymer actuators. *Smart Materials and Structures* **2012,** 21, (5), 055012.
25. Jeon, S.-J.; Hauser, A. W.; Hayward, R. C., Shape-Morphing Materials from Stimuli-Responsive Hydrogel Hybrids. *Accounts of Chemical Research* **2017,** 50, (2), 161-169.
26. Foroughi, J.; Spinks Gm Fau - Wallace, G. G.; Wallace Gg Fau - Oh, J.; Oh J Fau - Kozlov, M. E.; Kozlov Me Fau - Fang, S.; Fang S Fau - Mirfakhrai, T.; Mirfakhrai T Fau - Madden, J. D. W.; Madden Jd Fau - Shin, M. K.; Shin Mk Fau - Kim, S. J.; Kim Sj Fau - Baughman, R. H.; Baughman, R. H., Torsional carbon nanotube artificial muscles. (1095-9203 (Electronic)).
27. Reyssat, E.; Mahadevan, L., Hygromorphs: from pine cones to biomimetic bilayers. *Journal of The Royal Society Interface* **2009,** 6, (39), 951-957.
28. Shin, B.; Ha, J.; Lee, M.; Park, K.; Park, G. H.; Choi, T. H.; Cho, K.-J.; Kim, H.-Y., Hygrobot: A self-locomotive ratcheted actuator powered by environmental humidity. *Science Robotics* **2018,** 3, (14), eaar2629.
29. Alexander, S. L. M.; Ahmadmehrabi, S.; Korley, L. T. J., Programming shape and tailoring transport: advancing hygromorphic bilayers with aligned nanofibers. *Soft Matter* **2017,** 13, (33), 5589-5596.
30. Alexander, S. L. M.; Korley, L. T. J., Tunable hygromorphism: structural implications of low molecular weight gels and electrospun nanofibers in bilayer composites. *Soft Matter* **2017,** 13, (1), 283-291.
31. Armon, S.; Efrati, E.; Kupferman, R.; Sharon, E., Geometry and Mechanics in the Opening of Chiral Seed Pods. *Science* **2011,** 333, 1726-1730.
32. Erb, R. M.; Sander, J. S.; Grisch, R.; Studart, A. R., Self-shaping composites with programmable bioinspired microstructures. *Nature Communications* **2013,** 4, 1712.
33. Wang, Z. J.; Zhu, C. N.; Hong, W.; Wu, Z. L.; Zheng, Q., Programmed planar-to-helical shape transformations of composite hydrogels with bioinspired layered fibrous structures. *Journal of Materials Chemistry B* **2016,** 4, (44), 7075-7079.
34. Hu, Z.; Zhang, X.; Li, Y., Synthesis and application of modulated polymer gels. *Science* **1995,** 269, (5223), 525-527.
35. Fels, I. G., Hydration and density of collagen and gelatin. *Journal of Applied Polymer Science* **1964,** 8, (4), 1813-1824.

36. Schindelin, J.; Arganda-Carreras, I.; Frise, E.; Kaynig, V.; Longair, M.; Pietzsch, T.; Preibisch, S.; Rueden, C.; Saalfeld, S.; Schmid, B., Fiji: an open-source platform for biological-image analysis. *Nature methods* **2012,** 9, (7), 676.
37. Flory, P. J., *Principles of Polymer Chemistry*. Cornell University Press: Ithaca, NY, 1953.
38. Gorgieva, S.; Kokol, V., Collagen-vs. gelatine-based biomaterials and their biocompatibility: review and perspectives. In *Biomaterials applications for nanomedicine*, IntechOpen: 2011.
39. El-Tahlawy, K.; Venditti, R. A.; Pawlak, J. J., Aspects of the preparation of starch microcellular foam particles crosslinked with glutaraldehyde using a solvent exchange technique. *Carbohydrate Polymers* **2007,** 67, (3), 319-331.
40. Yapel, R. A.; Duda, J. L.; Lin, X.; von Meerwall, E. D., Mutual and self-diffusion of water in gelatin: experimental measurement and predictive test of free-volume theory. *Polymer* **1994,** 35, (11), 2411-2416.
41. Bohidar, H. B.; Jena, S. S., Kinetics of sol–gel transition in thermoreversible gelation of gelatin. *The Journal of Chemical Physics* **1993,** 98, (11), 8970-8977.
42. Treloar, L. R. G., *The Physics of Rubber Elasticity*. Oxford University Press: Oxford, 1975.

CHAPTER 4: PH RESPONSIVE CYCLIC GELATIN ACTUATORS

Hanzly, L.E. and Barone, J.R., (2019). pH Responsive Cyclic Gelatin Actuators

pH Responsive Cyclic Gelatin Actuators

*Laura E. Hanzly[1] and Justin R. Barone[1-3]**
[1]Biological Systems Engineering, [2]Macromolecules Innovation Institute, [3]Center for Soft Matter and Biological Physics
Virginia Tech
Blacksburg, VA 24061

Abstract

Soft actuators are designed to move in repsonse to environmental stimuli. Here, a biocompatable and biodegradable soft actuator designed from gelatin bilayers that moves in response to changes in pH is presented. The gelatin bilayer is consists of one layer derived from Type A gelatin and one layer dervied from Type B gelatin. The bilayer system bends/actuates when one layer swells to a creater degree than the other layer. Type A and Type B gelatin have different isoelectric points, therefore their gel layers will swell to different degrees when placed in various pH solutions. Maxiumum bilayer bending occurs at pH 10, when the Type B gelatin layer swells significantly more than the Type A layer. Cyclic actuation can be achieved via placing bent bilayers in a minimum of .01M NaCl solution for 24 hours. These results show the ability to use the unique properties of different sources of gelatin to design simple soft actuators.

*To whom correspondence should be addressed, jbarone@vt.edu

Introduction

The role of robotics in industry and society is undergoing a revolution. There is increasing demand for soft robots that are deformable, adaptable to changes in the environment, biocompatible, and biodegradable.[1] This is in contrast to traditional robots that are rigid, heavy, and programmed to perform a specific task. Further advancement in the field of soft robotics relies on the development of novel soft actuators made from compliant materials, i.e. elastic components that convert energy from external stimuli into mechanical motion.[2] Current examples of soft actuating materials include electroactive polymers, polyelectrolyte gels, shape memory polymers, and ionic liquids and polymers that are sensitive to environmental changes in temperature, pH, light, solvent, electric field, and humidity.[2, 3,4]

A common soft actuator/sensor design consists of polymer bilayers. Movement, in this case bending, is the result of an active layer swelling more than a passive layer in response to a stimulus (Figure 1).[4] This type of bilayer design has been observed in nature, a specific example being pine cones.[5] The bilayer structure of the scales within pine cones are responsible for the opening of the cones in dry conditions and closing of the cones in wet conditions. Motivated by nature, several synthetic versions of soft actuating bilayers have been developed using a variety of the aforementioned stimuli responsive soft materials.[6,7,8,9,10,11] Amongst the materials used for bilayer soft actuators are hydrogels because of their ability to undergo large volume changes and respond to several different types of stimuli.[4]

Present challenges to soft actuator design lie in the high cost of materials and tedious fabrication processes.[12] In particular, responsive hydrogels often require complex

fabrication techniques such as photolithography[13], spatially separated crosslinkers[14], or ionoprinting[15] causing mass production to be difficult and expensive.[16] Here we present an inexpensive, cyclic hydrogel soft actuator made from gelatin bilayers. Gelatin is a denatured form of collagen proteins and has been used for a variety of biomedical and pharmaceutical applications due to its biocompatibility, biodegradability, and low cost.[17,18,19] Gelatin hydrogels can also be easily molded into various shapes and forms making it a cost-effective material to manipulate.

Depending on the collagen processing conditions, gelatin can exhibit drastically different ionic properties.[17,20,21] For example, the alkaline hydrolysis of collagen derived from bovine skin results in an acidic gelatin, called Type B gelatin, with an isoelectric point (pI) of 5.0. Alternatively, Type A gelatin is basic gelatin with pI=7.0-9.0 that is produced from the acid hydrolysis of collagen from porcine skin. Gelatin hydrogels show pH responsive swelling behavior, meaning the swellability of the hydrogel is highly dependent on the pH of the solution the hydrogel is placed in.[20,22,23] For pH values close to the isoelectric point, the gelatin hydrogel exhibits a decreased swelling capacity because of the net neutral charge of the proteins within the hydrogel network. For pH values away from the pI, gelatin hydrogels display large swelling due to the electrostatic repulsion of many like charges on the collagen molecules.

It is hypothesized that the pI difference between Type A and Type B gelatin would allow for the creation of a soft actuating bilayer, with one layer made from Type A gelatin and the other layer made from Type B gelatin, which responds to changes in pH. Bending of the actuator is dependent on the swelling difference between the gelatin layers, with maximum bending occurring when the actuator is subjected to a pH near the pI of Type A

gelatin. Bending of the actuator can be reversed with the addition of salt and the cycle repeated. This results in a novel cyclic soft actuator that is easy to manufacture, economical, and completely biodegradable and biocompatible.

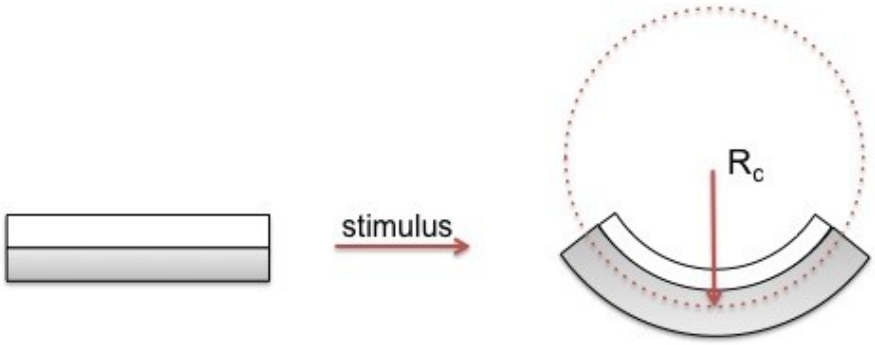

Figure 1. Schematic of bilayer actuator design. The active layer (gray layer) swells more than the passive layer (white layer) causing the entire system to bend. Bending is quantified by measuring the radius of curvature, R_c.

Materials and Methods

Single Layer Gels. Type A (G2500) and Type B (G9382) gelatin were purchased from Sigma Aldrich (St. Louis, MO). Single layer gelatin gels were prepared by first dissolving 20 wt% of either Type A or Type B gelatin in deionized water at 40°C. Once dissolved, the gelatin solution was placed in a vacuum oven to remove air bubbles. 5 ml of gelatin solution was then poured into a circular (5.5 cm diameter) silicone mold and allowed to dry for 10 minutes. Gelatin gels were cut and removed from silicone molds using a 4.4 cm diameter circular metal cutter.

Rheology. Gelatin gels were swollen in deionized water for 48 hrs before rheology testing. Oscillatory shear experiments were performed using 25 mm parallel plates on a DR3000 rheometer (TA Instruments, New Castle, DE). An applied strain of 0.1%, well within the viscoelastic region for Type A and Type B gelatin, was used for frequency

sweeps that ranged from 0.1 to 100 rad/s. Gap height between the plates varied based on sample thickness. Experiments were performed at room temperature and results reported as average elastic modulus, G', ± standard error.

pH Swelling Studies. Single layer gels were swollen in pH 2, 4, 6, 8, 10, and 12 solutions. pH solutions were prepared by adding either 1M NaOH or 1M HCl to 500 ml of distilled water. Gels were weighed after swelling for 48 hrs and then placed on Teflon sheets to dry. The dry weight of the gels was recorded after 48 hrs of drying. Swelling studies were performed in triplicate and results reported as average swelling ± standard error. Swelling ratios for pH 2 and 12 were not reported as gelatin gels disintegrated at these pH values.

Bilayer Gels. Bilayer gels were formed by depositing single layers of gelatin on top of one another. 5 ml of 20 wt% Type B gelatin solution (as previously described) was first poured into the silicone mold. After allowing this first layer to dry for 10 minutes, 5 ml of 20 wt% Type A gelatin solution was poured directly on top of the Type B gelatin layer in the silicone mold. Once dry, gelatin bilayers were cut and removed from the mold using the same 4.4 cm circular cutter used to prepare single layer gels.

Bilayer Swelling and Curvature Measurements. Gelatin bilayers were swollen in the same pH solutions as used for the single layers for 48 hrs. Bilayers were then removed from the solution and photographed. The radius of curvature, R_c, of the bilayers was measured using Fiji software. Experiments were performed in triplicate and average curvature, $\kappa=1/R_c$, ± standard error reported for each pH.

Cyclic Actuation Experiments. Gelatin bilayers were first swollen in pH 6 solution for 48 hrs. The bilayers were then placed in pH 10 solution for another 48 hrs. NaCl (Sigma

Aldrich) was then directly added and dissolved into the pH 10 solution beakers. Bilayers were incubated in the salt solutions for 24 hrs after which they were placed in fresh pH 10 solution for another 48 hrs. At each pH change and salt addition, the bilayers were removed from solution and photographed in order to measure their curvature. Experiments were performed in triplicate and average curvature ± standard deviation reported for each salt concentration.

Results and Discussion

Individual Layer pH Swelling Studies. Type A gelatin and Type B gelatin single layer gels are placed in solutions of varying pH to determine the swelling differences at different pH (Figure 2). The equilibrium volume swelling ratio, Q, is defined as the ratio of the total swollen volume attainable (polymer + water solvent), V_T, to the dry polymer volume, V_p:

$$Q = \frac{V_T}{V_p} = \frac{1}{v_p} = \frac{w_w \rho_{gel}}{w_d \rho_T} \qquad (1)$$

where ν_p is the polymer volume fraction in the water swollen hydrogel.[24] Q is found from the the swollen weight of the gel, w_w, the dry weight of the gel, w_d, the density of the gel (ρ_{gel}=1.34 g/cm^3 for gelatin[25]), and the total density of the water swollen gelatin, ρ_T. ρ_T can be calculated from:

$$\rho_T = \left[\left(\frac{1}{\rho_{gel}} * \frac{w_d}{w_w}\right) + \frac{1}{\rho_w}\left(1 - \frac{w_d}{w_w}\right)\right]^{-1} \qquad (2)$$

where ρ_w=0.997 g/cm^3 is the density of water at room temperature. Type B single layer gels depict a minimum Q around pH 6 which is close to Type B's reported pI of 5. Type A single layer gels show minimum Q at pH 10, which is near its pI of 9. Both gelatin types show increases in swelling ratio at pH values away from their respective pIs.

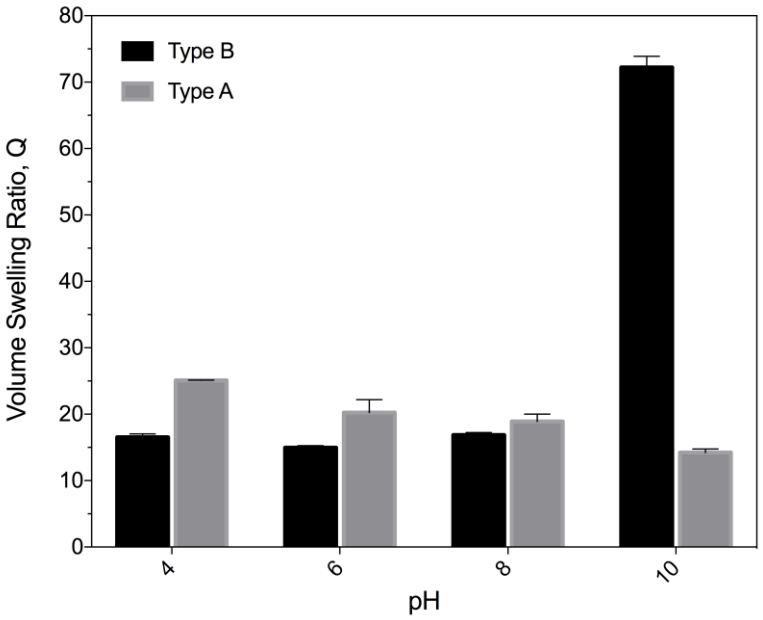

Figure 2. Average volume swelling ratio, Q, of Type A and Type B gelatin layers at various pH.

Overall, Type B gelatin layers demonstrate a greater capacity to swell to large volumes in comparison to Type A gelatin layers. Comparing both gelatins at 5 pH units from the pI, Q_{max}=72 for Type B gelatin at pH=10 and Q_{max}=25 for Type A gelatin at pH=4. Rheology experiments show Type A gelatin single layers have almost three times as large an elastic modulus, G', as Type B layers, at neutral pH and room temperature and the reported gel strength of Type A is higher than Type B gelatin (Table 1). Since $G'=\rho_T RT/M_c$, where R is the gas constant, T is the absolute temperature, and M_c is the molecular weight between crosslinks in the gel, the higher G' for Type A gelatin means that it is more crosslinked compared to Type B gelatin.[26] Gelatin physically crosslinks so these are not covalent crosslinks.[27] G' and Q are inversely proportional, which can be found by inserting the $G' \propto 1/M_c$ relationship into the Flory-Rehner theory (for high swell

ratios it approximates as $G' \sim Q^{-5/3}$).[28, 29] The higher crosslink density for Type A gelatin would limit its ability to swell relative to the lower crosslink density in Type B gelatin.

Table 1. Properties of Type A and Type B Gelatin.

Gelatin	Reported PI	Reported Gel Strength (Bloom)	Measured G' (Pa)
Type A	7-9	~300 g	6524.49 ± 200.63
Type B	4.7-5.2	~225 g	2323.38 ± 106.92

Bilayer pH Swelling Studies. Bilayer actuating gels were fabricated with one layer consisting of Type A gelatin and the other layer consisting of Type B gelatin. The gelatin bilayers showed different degrees of curvature depending on the pH of the swelling solution (Figure 3a,b). Bilayer curvature depends on the swelling difference between the Type A and Type B gelatin at the applied solution pH, which can be found from Figure 2 (Figure 3b). A comparison of the volume swelling ratios between the two layers, Q_p/Q_a, of the bilayers was performed at pH values 4,6, 8, and 10 where Q_p is the volume swell ratio of the passive layer and Q_a is the volume swell ratio of the active layer. For bilayers swelled in pH=4, 6, and 8, the Type A gelatin layer is considered the active layer because it swells more than the Type B gelatin layer, which is the passive layer. At pH=10, the Type B gelatin layer acts as the active layer (swells more) and the Type A gelatin layer acts as the passive layer (swells less). When $Q_p/Q_a \rightarrow 1$ there is not enough swelling difference between the layers for the bilayer to bend, which is what happens at pH=9.[5] As $Q_p/Q_a \rightarrow 0$, there is significant difference between layer swelling and measurable bilayer bending with maximum curvature occurring at pH=10. Bilayers in which Type A gelatin is the active layer show less curvature than bilayers with Type B gelatin as the active layer due to Type

A gelatin not being able to swell to the same degree as the Type B gelatin over the applied pH range.

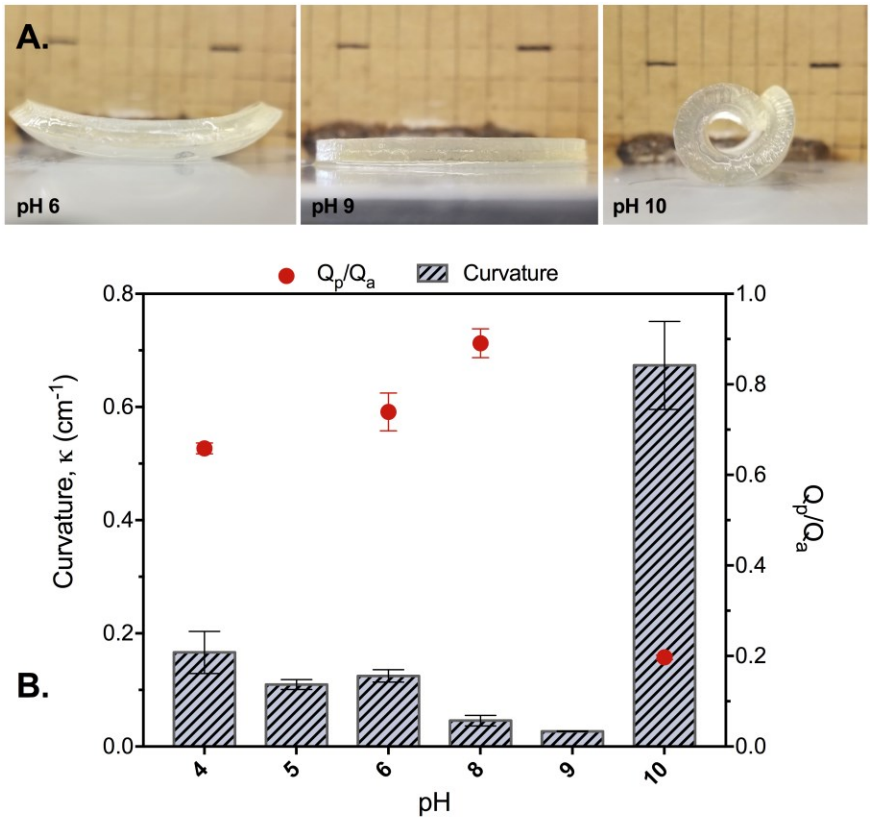

Figure 3. Curvature of bilayers at various pH. (a) Pictures of gelatin bilayers swollen for 48 hours at pH 6, 9, and 10. (b) Average curvature for bilayers after 48 hours of swelling in different pH solutions. Q_p/Q_a is the volume swell ratio of the passive layer compared to the active layer. For pH values 4,6, and 8, Type A gelatin swells more than Type B and is used as the active layer in calculations. At pH 10, Type B gelatin is the active layer because it swells more than the Type A layer.

Cyclic Bilayer Actuation. Reversible actuation would result in the bilayer completing a cycle and performing a net amount of work. Repeating the cycle over and over again would result in a soft machine. For example, a major drawback of some soft actuators is that their shape change is irreversible.[30] Gelatin bilayer actuation cannot be reversed by placing the gelatin bilayer in a different pH solution. For instance, the curvature displayed

by a gelatin bilayer at pH=10 cannot be reversed by placing the bilayer in a pH=9 or pH=6 solution. Actuation can be reversed, however, when the bilayer is placed in a solution of higher ionic strength (Figure 4). Cyclic actuation, going from flat to highly curved to flat again, is achieved by taking bilayers that were flat at pH=6, placing them into pH=10 solutions to completely bend, and then placing the bent bilayers in solutions of NaCl at various molarity to unbend. The cycle could be continued by taking the bilayers out of salt solutions and placing them back into pH=10 solutions. The highest concentration of NaCl tested, 0.1M, restricted the degree of curvature the bilayer returned to when placed back into pH=10 solution. The lowest concentration of NaCl tested, 0.01M, was not strong enough to return the bilayer to its initial curvature at pH=6. At 0.05M NaCl, the bilayers unbend to their initial curvature at pH=6 and are also able to bend back to their pH=10 curvature when removed from the 0.05M NaCl solution and placed back into a pH=10 solution.

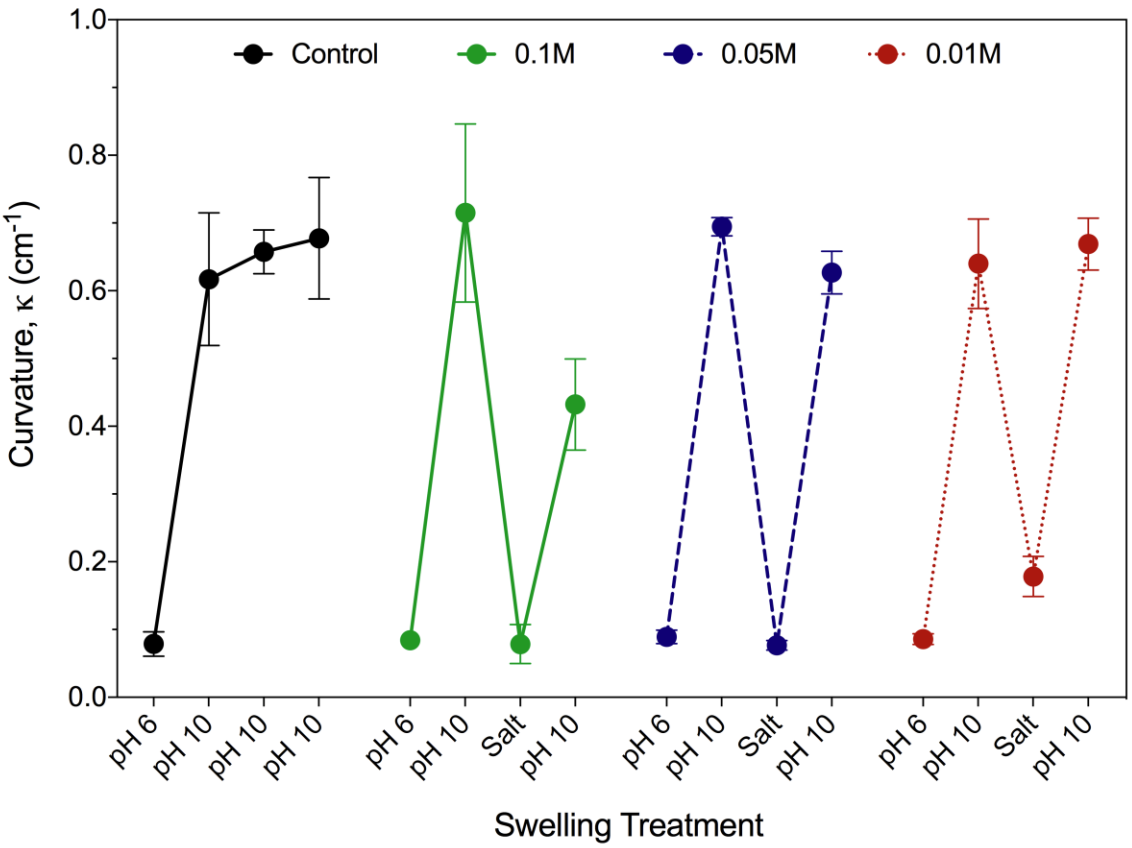

Figure 4. Cyclic actuation of gelatin bilayers. Gelatin bilayers are first swollen in pH=6 where they are relatively flat. Bilayers are then placed at pH=10 where they show maximum curvature. Bilayers are then placed in either 0.1M, 0.05M, or 0.01M NaCl solutions so the individual layers contract and the bilayer unbends. Finally, bilayers are placed back into pH=10 solutions. The control group was kept in a constant solution of pH=10.

Bilayer swelling and bending is a relatively slow process, as it relies on the diffusion of water into the gelatin matrix. The total time for one cycle is 120 hrs (48 hrs in pH=6, 48 hrs in pH=10, and 24 hrs in salt). Swelling time could be reduced by producing thinner bilayers or by using layers that contain less wt% gelatin, depending on application needs. This cyclic system is unusual in that both layers can act as the active layer at some point during the cycle. Most hydrogel bilayer systems have actuation based on one layer that serves as the active layer while the other layer is the permanent passive layer.[10] In this

system, the Type A gelatin layer acts as the active layer at pH=6 and the Type B gelatin is the active layer at pH=10. Having a bilayer where either layer can act as the active layer while the other layer acts as a temporary passive layer allows for the bilayer to actuate to a larger number of stimuli than traditional bilayers with one permanent active layer.

Conclusions

An actuating gelatin bilayer system was created by utilizing the differences in physical properties, such as pI and gel strength, of gelatin formed from different sources and processing conditions. Type A and Type B gelatin layers swelled to different capacities at different pH values, resulting in a bilayer system that bent to different degrees of curvature depending on the pH of the swelling solution. The bilayer system had a maximum curvature at pH=10, when the volume swelling difference between the two layers was the highest. Cyclic actuation was achieved by placing bilayers in NaCl solutions, which caused highly swollen layers to contract and the bilayer to become flat. The system was comprised only of gelatin, making it completely biodegradable and biocompatible as well as inexpensive to fabricate. Different gelatin types with different gel strengths can be used to tailor the response of the current system. Applications of such a system could involve loading drugs, enzymes, flavor compounds, etc. into one or both layers of the system. Swelling in response to pH would allow for the release of one drug from the temporary active layer while another drug remains loaded in the temporary passive layer, which could be released at a later time.

Acknowledgements

Laura Hanzly was supported by a Graduate Teaching Scholarship (GTS) at Virginia Tech.

References

1. Majidi, C., Soft robotics: a perspective—current trends and prospects for the future. *Soft Robotics* **2014,** 1, 5-11.
2. Asaka, K.; Okuzaki, H., *Soft Actuators: Materials, Modeling, Applications, and Future Perspectives*. Springer: 2014.
3. Bauer, S.; Bauer-Gogonea, S.; Graz, I.; Kaltenbrunner, M.; Keplinger, C.; Schwödiauer, R., 25th Anniversary Article: A Soft Future: From Robots and Sensor Skin to Energy Harvesters. *Advanced Materials* **2014,** 26, 149-162.
4. Gracias, D. H., Stimuli responsive self-folding using thin polymer films. *Current Opinion in Chemical Engineering* **2013,** 2, 112-119.
5. Reyssat, E.; Mahadevan, L., Hygromorphs: from pine cones to biomimetic bilayers. *Journal of The Royal Society Interface* **2009,** 6, 951-957.
6. Cheng, F.; Yin, R.; Zhang, Y.; Yen, C.-C.; Yu, Y., Fully plastic microrobots which manipulate objects using only visible light. *Soft Matter* **2010,** 6, 3447-3449.
7. Xie, T.; Xiao, X.; Cheng, Y. T., Revealing triple-shape memory effect by polymer bilayers. *Macromolecular Rapid Communications* **2009,** 30, 1823-1827.
8. Bae, C. Y.; Park, J. H.; Kim, E. Y.; Kang, Y. S.; Kim, B. K., Organic–inorganic nanocomposite bilayers with triple shape memory effect. *Journal of Materials Chemistry* **2011,** 21, 11288-11295.
9. Li, X.; Cai, X.; Gao, Y.; Serpe, M. J., Reversible bidirectional bending of hydrogel-based bilayer actuators. *Journal of Materials Chemistry B* **2017,** 5, 2804-2812.
10. Cheng, Y.; Ren, K.; Yang, D.; Wei, J., Bilayer-type fluorescence hydrogels with intelligent response serve as temperature/pH driven soft actuators. *Sensors and Actuators B: Chemical* **2018,** 255, 3117-3126.
11. Bassik, N.; Abebe, B. T.; Laflin, K. E.; Gracias, D. H., Photolithographically patterned smart hydrogel based bilayer actuators. *Polymer* **2010,** 51, 6093-6098.
12. Rus, D.; Tolley, M. T., Design, fabrication and control of soft robots. *Nature* **2015,** 521, 467.
13. Shim, T. S.; Kim, S. H.; Heo, C. J.; Jeon, H. C.; Yang, S. M., Controlled origami folding of hydrogel bilayers with sustained reversibility for robust microcarriers. *Angewandte Chemie* **2012,** 124, 1449-1452.
14. Kim, J.; Hanna, J. A.; Byun, M.; Santangelo, C. D.; Hayward, R. C., Designing responsive buckled surfaces by halftone gel lithography. *Science* **2012,** 335, 1201-1205.
15. Palleau, E.; Morales, D.; Dickey, M. D.; Velev, O. D., Reversible patterning and actuation of hydrogels by electrically assisted ionoprinting. *Nature communications* **2013,** 4, 2257.

16. Velders, A. H.; Dijksman, J. A.; Saggiomo, V., Hydrogel actuators as responsive instruments for cheap open technology (HARICOT). *Applied Materials Today* **2017,** 9, 271-275.
17. Tabata, Y.; Ikada, Y., Protein release from gelatin matrices. *Advanced drug delivery reviews* **1998,** 31, 287-301.
18. Djagny, K. B.; Wang, Z.; Xu, S., Gelatin: a valuable protein for food and pharmaceutical industries. *Critical reviews in food science and nutrition* **2001,** 41, 481-492.
19. Arvanitoyannis, I. S., Formation and properties of collagen and gelatin films and coatings. In *Protein-based films and coatings*, CRC Press: 2002; pp 289-318.
20. Hafidz, R.; Yaakob, C. M.; Amin, I.; Noorfaizan, A., Chemical and functional properties of bovine and porcine skin gelatin. *International Food Research Journal* **2011,** 18, 813-817.
21. Young, S.; Wong, M.; Tabata, Y.; Mikos, A. G., Gelatin as a delivery vehicle for the controlled release of bioactive molecules. *Journal of controlled release* **2005,** 109, 256-274.
22. Gupta, P.; Vermani, K.; Garg, S., Hydrogels: from controlled release to pH-responsive drug delivery. *Drug discovery today* **2002,** 7, 569-579.
23. Qiao, C.; Cao, X.; Wang, F., Swelling behavior study of physically crosslinked gelatin hydrogels. *Polymers and Polymer Composites* **2012,** 20, 53-58.
24. Rubinstein, M.; Colby, R. H., *Polymer Physics*. Oxford University Press: Oxford, 2003.
25. Fels, I. G., Hydration and density of collagen and gelatin. *Journal of Applied Polymer Science* **1964,** 8, 1813-1824.
26. Usta, M.; Piech, D. L.; MacCrone, R. K.; Hillig, W. B., Behavior and properties of neat and filled gelatins. *Biomaterials* **2003,** 24, 165-172.
27. Bigi, A.; Panzavolta, S.; Rubini, K., Relationship between triple-helix content and mechanical properties of gelatin films. *Biomaterials* **2004,** 25, 5675-5680.
28. Flory, P. J., *Principles of Polymer Chemistry*. Cornell University Press: Ithaca, NY, 1953.
29. Treloar, L. R. G., *The Physics of Rubber Elasticity*. Oxford University Press: Oxford, 1975.
30. van Manen, T.; Janbaz, S.; Zadpoor, A. A., Programming the shape-shifting of flat soft matter. *Materials Today* **2018,** 21, 144-163.

CHAPTER 5: CONCLUSIONS

The overall goal of this work was to explore the use of proteins as a biodegradable, sustainable material in composites and as functional materials. The proteins wheat gluten and gelatin were used because of their low cost, availability, and unique capabilities. When hydrolyzed with trypsin, wheat gluten is capable of self-assembling into β-sheet structures. This self-assembly process was explored as a potential mechanism for *in situ* nanofiller formation in polymer matrices. Gelatin can undergo large volume changes when placed in a compatible solution due to its ability to form hydrogels. Macroscopic volume changes in gelatin were utilized in the design of a biodegradable and biocompatable soft actuator.

In Chapter 2, trypsin hydrolyzed wheat gluten (THWG) proteins were self-assembled in aqueous polyvinyl alcohol (PVA). Increased solution viscosity impacted the rate of THWG self-assembly, as determined by FTIR. Of the three different molecular weight PVAs used, THWG showed the fastest self-assembled kinetics in the lowest molecular weight PVA. However this self-assembly rate was still slower in comparison to THWG self-assembly in pure water. THWG self-assembly in PVA forms anisotropic spikes, which eventually agglomerate into "pompons". These spikes and pompons are shaped differently from the fibrils THWG forms in water, however it was determined that all THWG structures were formed through the same hydrophobic self-assembly mechanism. These results show that THWG self-assembly in aqueous polymer matrices could be used to form a biobased, multi-phase nanocomposite.

In Chapters 3 and 4, gelatin was used to create hydrogel bilayer soft actuators. Gelatin bilayer actuation was achieved through swelling differences between the two layers when placed in water. Bilayer curvature reached its maximum when the swelling of the passive layer was approximately 60% of the swelling of the active layer. Adding water-soluble pre-gelatinized starch to the active layer of the bilayer system increased active layer swelling and bilayer curvature. Treating starch-filled gelatin bilayers with the enzyme α-amylase removed the increased bilayer curvature. This demonstrated the ability of the

gelatin bilayer actuating system to be cyclic by first bending in the presence of water/starch and then unbending when removed from water or treated with α-amylase.

A third gelatin bilayer actuating system was designed to respond to changes in pH. This system made use of the difference in physical properties between Type A and Type B gelatin. Type A and Type B gelatin have different isoelectric points, therefore they swell to different degrees at a given pH. Maximum curvature occurred at pH 10, where the volume swelling difference between the two layers was the greatest. Bilayers could be "unbent" by placing the bilayers in a NaCl solution. Overall, Chapters 3 and 4 show the potential for a gelatin bilayer soft actuator to be designed to respond to a variety of different stimuli and is an actuator comprised from biological material that could be tailored to fit application needs.

Future work would involve the optimization of both of the aforementioned projects. For example, while wheat gluten is a low cost protein, the trypsin enzyme used for hydrolysis is expensive would not be viable for industrial use. Examination of the potential self-assembly of acid hydrolyzed wheat gluten could be a cost-effective solution to this problem. In the case of gelatin bilayer actuators, actuation is on the time-scale of hours. In order to decrease the time it takes for actuation to occur, thinner gelatin layers could be constructed. Additionally, using a lower weight % of gelatin to form the gels would also decrease the time it takes for the layers to swell and therefore actuate. Overall, this dissertation demonstrates the numerous material applications of common proteins. In order to shift away from a society reliant on biopersistant synthetic polymers, novel sustainable materials research like the projects presented here must be funded and conducted.